University Library

MINERVA ACCESS

A gateway to Melbourne's research publications

Minerva Access is the Institutional Repository of The University of Melbourne

Author/s:
Ren, J;Zhang, L;San Nicolas, R

Title:
Degradation of Alkali-Activated Slag and Fly Ash Mortars under Different Aggressive Acid Conditions

Date:
2021-07-01

Citation:
Ren, J., Zhang, L. & San Nicolas, R. (2021). Degradation of Alkali-Activated Slag and Fly Ash Mortars under Different Aggressive Acid Conditions. Journal of Materials in Civil Engineering, 33 (7), https://doi.org/10.1061/(ASCE)MT.1943-5533.0003713.

Persistent Link:
https://hdl.handle.net/11343/292045

Degradation of alkali-activated slag/fly ash mortars under different aggressive acid conditions

Jie Ren[1], Lihai Zhang[1], Rackel San Nicolas[1*]

[1] Department of Infrastructure Engineering, the University of Melbourne, Victoria, 3010, Australia

Abstract

Acidic environments constitute serious chemical threats to concrete-like cementitious materials. The purpose of this study is to experimentally investigate the degradation of alkali-activated slag/fly ash mortars with different slag/fly ash ratios: 80/20, 60/40 and 40/60 in acidic environments. Mortar samples were exposed to three different types of aggressive acidic solutions: phosphoric acid, sulphuric acid and a mixture of phosphoric acid and sulphuric acid maintained at a constant pH value of 2.5 ± 0.5 for a period of 150 days. Results showed that in the case of alkali-activated mortars, the aggressivity of the phosphoric acid alone is greater compared to the other acidic solutions. An optimum ratio of slag/fly ash was identified as a higher resistance against the three types of acidic environments studied here. Further, the degradation process of alkali-activated mortars seems to be different than the one observed on OPC, there are two clear stages. By using a combination of the Hill function and the Fick's second law a first model of degradation is proposed in this study. Finally, the results of theoretical analysis predicted that the degradation depth of alkali-activated slag/fly ash mortars exposed to sulphuric acid environment for 50 years could be reduced by about 52% - 60% compared to that of an OPC-based mortars.

Key words: Degradation depth, Alkali-activated slag/fly ash blended mortar, Sulphuric acid, Phosphoric acid, phosphoric and sulphuric acid mixture, Diffusion coefficient; Hill function

1. Introduction

A vast amount of Ordinary Portland cement (OPC)-based concrete has been used as construction materials for sewer and wastewater systems. However, the exposure of alkaline building materials such as OPC concretes to acid-rich aggressive environments leads to severe degradations [1, 2]. In the acid-rich environments, hydronium ions (H_3O^+) penetrate alkaline materials such as OPC-based concrete, inducing a significant pH reduction of pore solutions [3]. If the exposition continues, further dissolution and/or decomposition of various components such as Portlandite and C-S-H gel in the bulk materials

would occur and some calcium salts such as gypsum would be formed, worsening many mechanical properties, such as reduced compressive and flexural strength [4-7]. Thus the service life of concretes is reduced and considerable expenditure for repair and maintenance occurs as a result of degradations. It was predicted that it may cost the United States 390 billion dollars over the next two decades to repair current-in-service wastewater infrastructures [8] and the annual cost of operation and maintenance related to the wastewater infrastructure is more than 25 billion dollars [9].

Among all different types of concrete degradation caused by acid-laden sewer environments such as silage effluent, the degradation of various cementitious materials resulting from chemical and biochemical sulphuric acid has been extensively investigated in the last few decades [8, 10-14]. However, phosphoric acid induced degradation of concretes due to the coexistence of hydroniums (H_3O^+) released from various acids and large concentration of phosphates has not been much investigated and the relevant research in this area is quite limited [8, 15-17]. The available literature compared the aggressiveness of phosphoric acid and citric acid but without exploring related mechanisms of phosphoric acid degradation process [16]. In addition, almost all of the current literature focuses on the effect of one single acid, e.g. sulphuric or nitric acid, on the degradation performances of alkaline cementitious materials without considering the possible different effects of mixed acids [18-24]. However, different acids usually coexist in sewage systems due to the presence of different anions such as sulphates, phosphates, nitrate etc. and hydroniums in acidic conditions [17]. Thus, an investigation of the degradation performance of cementitious materials exposed to mixed acid solutions which is closer to real-life situations is required to draw a more convincing conclusion.

Alkali-activated materials (AAMs) are a class of binders prepared using different precursors as raw materials instead of using OPC [25]. These precursors are mixed together with various alkaline activators to provide necessary strong alkaline conditions for dissolution of precursors and the condensation catalysing processes [26]. Currently, AAMs are considered as an appealing alternative to OPC-based materials due to their much lower carbon footprint and comparable mechanical properties [15, 27, 28] as compared to OPC-based binders. In addition, both the activation of calcium-rich slag or low-calcium materials, such as fly ash (FA) and metakaolin, can provide higher resistance to aggressive environments such as acid attacks than that of OPC-based binders [29, 30] due to their distinctive chemical compositions and microstructures [31, 32]. The major components for slag-based and fly ash (FA)-based binders are C-(A)-S-H ($CaO-Al_2O_3-SiO_2-H_2O$)-type gel and N-A-S-H (Na_2O-

Al_2O_3-SiO_2-H_2O)-type gel, respectively. It was showed that slag-based AAMs had a better performance compared to OPC-based peers under sulphuric acid and acetic acid attacks [33, 34]. The authors [33, 34] attributed this relatively high durability mainly to the lower Ca/Si ratio of the binder matrix because of the absence of $Ca(OH)_2$ (Portlandite) in the composition of this type of AAMs and an extremely low permeability. For FA-based AAMs, the main reaction product (N-A-S-H) is a three-dimensional highly crosslinking network with low Ca content, contributing to higher resistance in acid solutions as compared to OPC-based binders [34-37]. Furthermore, alkali-activated slag/fly ash (AASF) binders are becoming more appealing due to some favourable combinations of the properties that cannot be achieved by the activation of one single precursor [38-43]. A high degree of cross-linked binder displaying a coexistence of C-(A)-S-H and N-A-S-H [44], either present as a single phase or a hybrid-type gel known as C-(N)-A-S-H gel in some studies, was observed when slag and fly ash were mixed together [45]. According to Lloyd et al.[46], the addition of slag into the FA-based AAMs increased the resistance towards the sulphuric acid attack with a pH at 1.0. However, another literature [23] found that increasing slag contents has a negative impact on the resistance of FA-based AAMs due to a higher content of calcium which is unfavourable regarding the acid resistance. The seemingly controversial outcomes can be explained by considering different roles the C-A-S-H and N-A-S-H play in terms of acid resistance. C-A-S-H has a space-filling effect in the binder, leading to a reduced porosity as slag content increases [23, 47]. However, C-A-S-H contains more Ca than N-A-S-H type gel which makes it more susceptible towards acid attacks via decalcification process. Therefore, a trade-off between the amount of slag and FA used for making AASF samples is required to optimise the durability performance of AASF binders.

Currently, a main hurdle preventing AAMs from wider applications is the lack of data and reports on the long-term behaviour of these materials that can prove satisfactory durability throughout their overall life-cycles [48, 49]. In order to allow more rapid adoption of AAMs as an alternative to OPC-based binders, to get reliable results which can be used for the quantification of AAMs' long service life is critical [6, 14, 23, 24, 46, 50, 51]. Among many parameters, degradation depth provides useful information on rate-controlling processes of concrete materials. Therefore it is often used as a reliable indicator for corrosion kinetics and long-term risk predictions [46]. In some studies, degradation depth is also considered as 'altered depth', 'neutralization depth' or even 'corrosion depth' [52-55]. 'Degradation depth' is used in this study for consistency.

A few studies have been conducted to measure the degradation depths of OPC-based binder or AAMs after immersion in various acidic solutions and related degradation mechanisms were also proposed [3, 46, 53, 56-59]. The experiment work of Lloyd et al. [46] revealed that the degradation depth is a more reliable method to assess the degradation kinetics, particularly for AAMs compared to mass loss. According to the experimental results, a linear relationship between the degradation depth and exposure time indicates a chemical reaction-controlled process [60] whereas a linear increase in the degradation depth over the square root of time implies that the degradation is mainly controlled by diffusion [46].

Earlier, Kawai et al. [58] exposed OPC-based concrete to sulphuric acid solution with pH at 1.0 and 2.0 respectively to investigate the degradation of concrete specimens under acid fluid flow over sample surfaces. Their results showed that there is a positive linear relationship between the degraded depth and exposure time, indicating a chemical-controlled process. This is due to the removal of the degraded layer and calcium salts by fluid flow. Other relevant experimental studies also reported that, when immersed in nitric acid, a highly porous degraded layer providing little protection for acid ingress led to a higher degradation rate (almost linear increase in the degradation depth over time when the pastes were completely dissolvable). In comparison, a compact and dense layer rich in silica after degradation resulted in a lower rate of degradation [56].

In conclusion, the initial stage of degradation is usually a chemical-reaction controlled process due to direct reactions between cementitious binders and exposed acids. However, the later process can be either reaction-controlled (porous/no intact degraded layer or degraded layer erased by external forces) or diffusion-controlled (dense and intact degraded layer). It is clear that based on the experimental results and general trends provided by degradation depth development, long-term behaviours of cementitious binders subjected to acid attacks could be predicted [51]. However, related research on studying the degradation depth of AAMs or OPC-based binders exposed to phosphoric acid solutions and predicting their long-term performances [16, 61, 62] is quite rare.

Therefore, the purpose of this study is to investigate the degradation processes of different mixtures of AAMs, specifically AASF, with three slag/FA ratios under various acid conditions: phosphoric acid, sulphuric acid and a mixture of phosphoric acid and sulphuric acid. Degradation depth was used as the parameter to assess the degradation process and kinetics. A series of theoretical simulations were then

carried out to further predict the long-term degradation behaviours of AASF binders and to compare their behaviours with those of OPC-based peers.

2. Experimental methods

2.1. Materials

The chemical compositions and properties of the slag, specifically ground granulated blast furnace slag (denoted as 'GGBFS' hereafter) and fly ash both from Australia are shown in Table 1. GGBFS used has a specific gravity of 2,800 kg/m^3 and Blaine fineness of 410 ± 10 m^2/kg. The particle size range, determined by laser granulometric analysis, was 0.1–74 μm, with a d_{50} of 14 μm. The specific gravity and d_{50} of fly ash is 2200 kg/m^3 and 25 μm, respectively. The silica sand (milled quartz) as fine aggregate with a specific gravity of 2550 kg/m^3 and water absorption of 0.90 % was used. Commercial solid anhydrous sodium metasilicate powder (Na_2SiO_3) with a chemical composition of 49.1 % wt.% SiO_2 and 50.9 wt.% Na_2O (a molar ratio of SiO_2/Na_2O at 1.0) is supplied by Zeobond Pty. Ltd.

Table 1. Chemical compositions of the FA and GGBFS used, as determined by X-ray fluorescence.

Oxide (wt %)	SiO_2	TiO_2	Al_2O_3	Fe_2O_3	MnO	MgO	CaO	K_2O	P_2O_5	SO_3	LOI
GGBFS	31.00	0.49	13.96	0.32	0.33	6.33	40.92	0.31	0.01	2.17	2.11
FA	42.09	1.44	25.13	13.16	0.18	1.27	13.56	0.41	1.10	0.41	0.81

LOI is loss on ignition at 1,000 ℃.

Three sets of alkali-activated mortars were produced with different GGBFS/FA ratios, as shown in Table 2. The mortar samples were formulated using different water-to-binder ratios (w/b) and amounts of alkaline activator to reach similar target compressive strengths (around 60 ± 5 MPa) after 56-day curing before immersion in acidic solutions to obtain a meaningful comparison. These dosages have been identified as the most suitable formulation to promote acceptable setting times and desirable structural evolutions [44, 63]. The sand to binder ratio is 2:1 by weight for all sample mixes. The water used for mixing the mortar and preparing activator solutions was purified distilled water. The activator, anhydrous sodium metasilicate (Na_2SiO_3), was weighed and dissolved completely in distilled water followed by cooling down to room temperature at 23 ± 2 ℃ before addition. Mortar samples were cast and compacted into cylinder moulds (Φ 27.5 mm × H 55 mm) in two layers of equal height using a tamping rod followed by being vibrated via a vibrating table for another 2 minutes to release air bubbles. The specimens namely, 80Slag_20FA, 60Slag_40FA, were cured at room temperature (23 ± 2 ℃) with a plastic film covered on them for 24 hours before they were demoulded to minimize moisture loss. The

40Slag_60FA sample was cured under hydrothermal water bath conditions (temperature at 70 ℃, RH = 95 ± 5 %) in a laboratory-grade oven wrapped with a vacuum plastic bag for seven days. After that, they were taken out of the oven, cooled down at room temperature (23 ℃) and demoulded. After demoulding, all samples were sealed tightly and kept in ambient conditions (room temperature 23 ± 2 ℃) until the next stage of the experiment. The modified curing regime used for the 40Slag_60FA sample was employed to reach the target strength after 56 days [61]. A fully cured cylindrical sample is presented in Fig. 1(a).

Table 2. Mixture designs of the mortar samples tested in the study.

Sample ID	Specifications (Mix proportions)			
	GGBFS/FA ratio (%)[a]	Activator/Binder ratio (%)[a]	Water/Binder ratio[a]	Sand/Binder ratio[a]
80Slag_20FA	80:20	7.0	0.40	2:1
60Slag_40FA	60:40	7.5	0.38	2:1
40Slag_60FA	40:60	8.5	0.34	2:1

[a] All values are given as mass ratios.

Three aggressive acid solutions, namely phosphoric acid (diacid in aqueous solution), sulphuric acid (strong diprotic acid) and the phosphoric acid and sulphuric acid mixed solution were made by adding laboratory grade acids into distilled water. The pH of the three different acids was all manually controlled at around 2.5 ranging between 2.0 and 3.0. The phosphoric acid solution was made by diluting 1,000 times of the original analytical reagent phosphoric acid provided by Chem-supply (85% w/w, 1.71 g/mL) to 14.82 mM (0.085%, 0.015 mol/L). The sulphuric acid solution was prepared by diluting the original reagent grade sulphuric acid supplied by Scharlau, UN (95-97% w/w, 1.84 g/mL) with a 4,000-fold to 4.69 mM (0.005 mol/L, 0.024% w/w). The mixed acid was made by mixing the prepared phosphoric acid and sulphuric acid solution together with a 1:1 ratio in volume. The initial pH of the phosphoric and sulphuric mixed acid was slightly higher than the other two single acid solutions because phosphoric acid is partially ionised and its ionization would be, to some extent, inhibited by the complete dissociation of sulphuric acid. However, the hydronium ions which can be dissociated from the phosphoric and sulphuric mixed acid with volume ratio of 1:1 are readily available. Therefore, the phosphoric and sulphuric mixed acid can represent the scenario where phosphoric and sulphuric acid are mixed together with similar pH as the other two pre-mixed single acids. The details of the three acid solutions are shown in Table 3.

Table 3. The detailed information on the three aggressive acid solutions in which the samples were immersed for 150 days.

Sample ID	Acid solution types (pH = 2.5 ± 0.5)		
	Phosphoric acid	Sulphuric acid	Phosphoric + sulphuric acid
80Slag_20FA	14.83 mM	4.69 mM	7.42 mM (P) + 2.35 mM (S)
60Slag_40FA	14.83 mM	4.69 mM	7.42 mM (P) + 2.35 mM (S)
40Slag_60FA	14.83 mM	4.69 mM	7.42 mM (P) + 2.35 mM (S)

Note: 'P' and 'S' stands for reagent-grade phosphoric acid and sulphuric acid, respectively. Notation (mM: mmol/L).

2.2. Methods

Samples after 56 days of curing were fully immersed in the three acid solutions while keeping the solid surface/liquid volume ratio constant at 0.30 cm^{-1}. The vertical distance between liquid levels of the acid solution and top surfaces of the samples was kept no less than 10 mm to ensure a complete immersion which can minimize possible carbonation induced by CO_2 from the air. Each sample was supported on two plastic holders to maximize the contact area between the sample surface and acid solution shown in Fig. 1(b). To keep the pH of all acid solutions constant, the pH values were monitored using a portable pH-meter (PHM210 Radiometer, Australia) and solutions were renewed every day in the first 7 days followed by a gradually decreased frequency of renewals until the end of the experiment (after 7 days, the solutions were replaced every second day for 21 days and every 3 days for another 21 days. After 49 days, the acid solutions were renewed every 7 days until the end of the immersion period). The renewal frequency was pre-determined based on previous preliminary studies which indicated that the number of pH adjustment could be reduced as the immersion period proceeds [54]. Each time when the solutions were renewed, samples were also rinsed slightly with distilled flowing water for a few seconds to represent the actual practical conditions that construction materials might encounter in sewage systems [64]. The acid solutions were allowed to stand without any mixing to simulate the static environments observed in tanks and sewer pipes containing agro-industrial effluents [65].

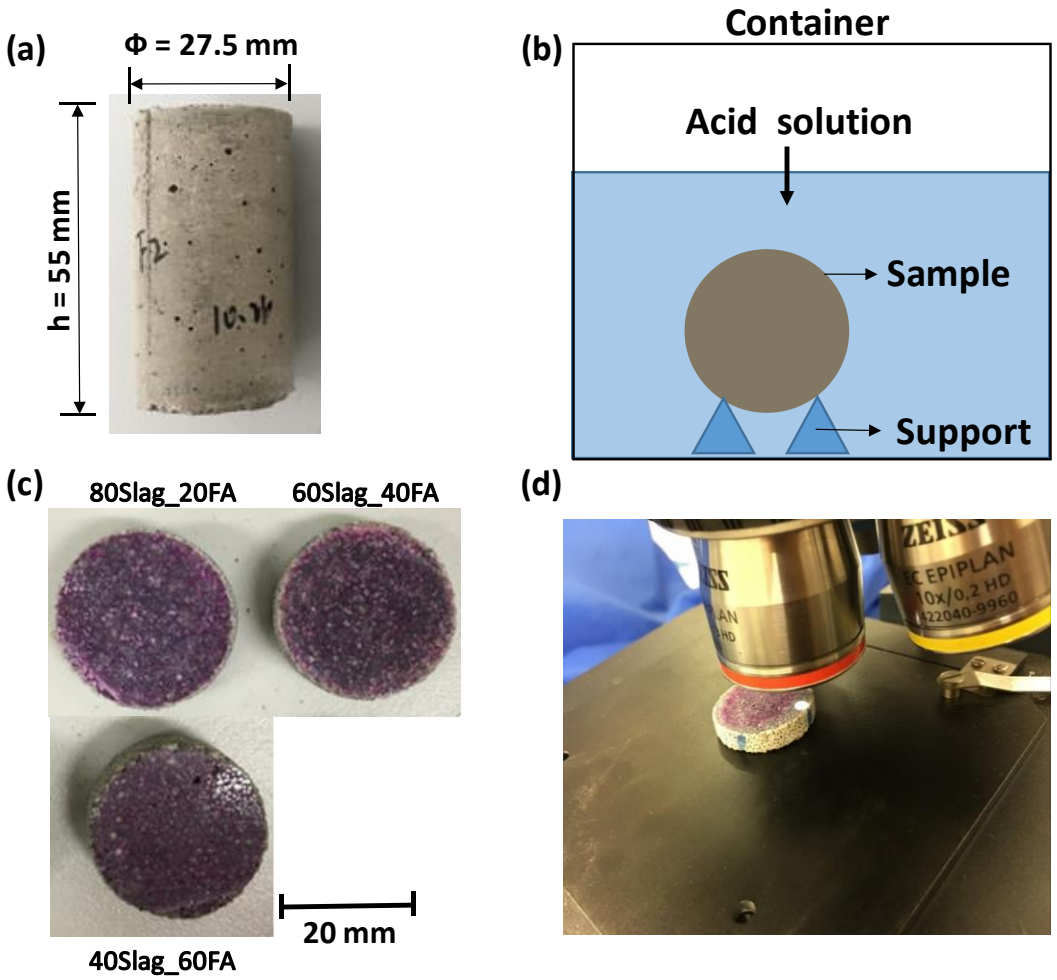


Fig. 1. The detailed experimental procedures: (a) A cylindrical sample used for the acid immersion; (b) A schematic representation of the experimental setups; (c) Cross sections of all sample mixes after 90-day immersion in sulphuric acid; (d) Measurement of degradation depths using an optical video-microscope after 7, 28, 56, 90, 120 and 150 days of immersion.

A simple description of all experimental details is shown in Fig. 1. Fig. 1(a) represents a cylindrical mortar sample after 56 days of curing. Fig. 1(b) shows the sample orientations for acid immersion test. Fig. 1(c) and (d) give information about the procedures of degradation depth measurements.

Compressive strength test was performed on cubic mortar samples (50 × 50 × 50 mm) in triplicates according to ASTM C109M [66] after 56-day curing prior to acid exposure.

The initial water absorption (%), volume of permeable voids (%) (VPV) and capillary sorptivity ($mm/min^{0.5}$) of all samples were obtained by taking related tests according to ASTM C642-06 [67] and ASTM C1585-04 [68]. All tests were conducted on cylinder samples (27.5 mm in diameter and 55 mm

in height) right after 56-day curing regime. Due to the preconditioning drying effect [69] on the alkali-activated binders, 70 ℃ was selected for oven-drying of the specimens until a constant mass was obtained. This process took about 4-5 days before reaching a constant mass. The 70 degree oven-drying temperature was used based on the study of Ismail et al.[69] because possible microstructural changes of AAM samples could happen under a relatively high temperature (e.g. 110 ℃) suggested by the ASTM C642-06 [69]. Water absorption and VPV provide information about total volumes of various voids. Capillary sorptivity is one of the most important microstructural properties that characterises the durability of materials because it reflects the tendency of binders to absorb and transmit water or other liquids by capillary action [6] during the initial stage of absorption. In this study, hydroniums in water penetrate into the samples along with the water ingress.

Degradation depth was measured using an optical microscope along the immersion process after 7, 28, 56, 90, 120 and 150 days of exposure, as an indicator of degradation kinetics. Three cylinders of each formulation were used to obtain the final averaged degradation depth. A disk of samples was cut perpendicularly to its axis by a diamond saw and then the disks were cleaned with water. In order to get a flat surface, each sample was polished on a sanding belt for 2 minutes with 120 grit sand paper and then dried in ambient environment with compressed air. A phenolphthalein solution (1 g phenolphthalein dissolved in 70 mL 95 % ethanol solution mixed with 100 mL distilled water) was then sprayed onto the newly-cut flat plane sections as an indicator of the degradation depth. The colourless area indicates that the pH dropped to below 8.3 and is considered as degraded [28]. The magenta-coloured region indicating a pH higher than 10.0 is considered as no damage occurred. There are some areas with light magenta/pink colour referring to a pH between 8.3-10.0. In this study, only the uncoloured area is regarded as the degraded part. Pictures were then taken by the optical-video microscope and processed in MATLAB to precisely calculate the apparent degradation depth (*ADD*). The diameter was also measured at the same time for each testing interval as the diameters of cross section was decreased due to partial dissolution of samples during the acid deterioration process [54]. The dissolved depth (*DD*) can be deduced from the formula: $\mathrm{DD} = (\varphi_{ini} - \varphi_t)/2$ where φ_{ini} is the initial diameter of the samples and φ_t is the diameter at each time interval t. The total degradation depth (*TDD*) is a numerical sum of *ADD* and *DD*. A presentation of the identification of different depths is shown in Fig. 2.

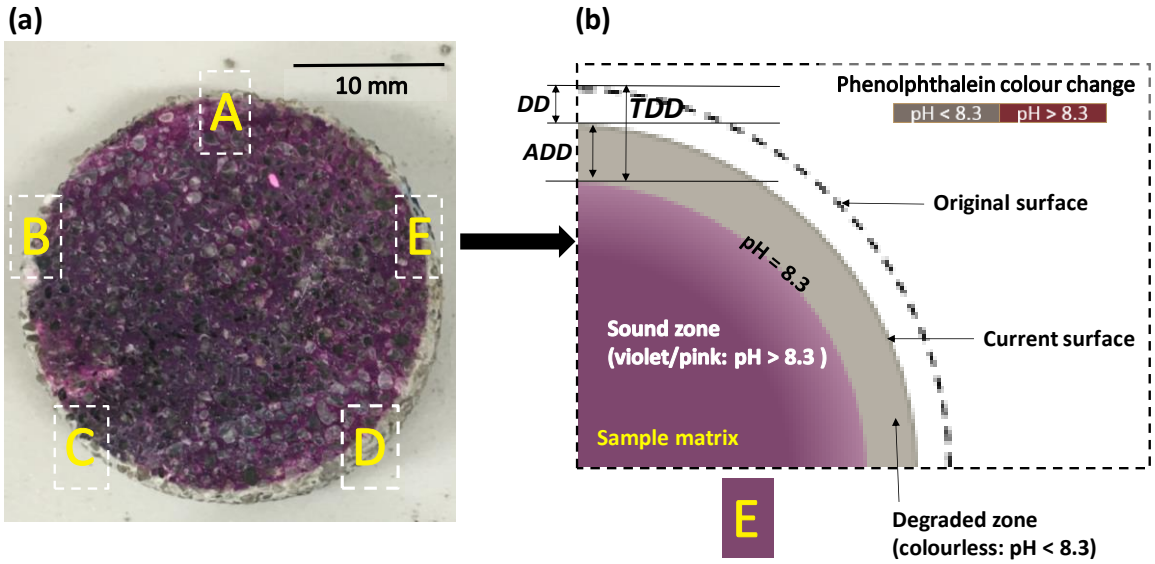


Fig. 2. Definitions of different parts involved in the degradation depth measurement. (a) A slice cut from a sample after 120-day immersion in the phosphoric and sulphuric mixed acid with phenolphthalein sprayed on the surface; (b) A schematic representation showing the identification of degradation depth at region 'E' (*TDD* - Total Degradation Depth, *ADD* - Apparent Degradation Depth, *DD* - Dissolved Depth). 'A'-'E' are several points selected around the peripheries of the sample for ADD measurements.

3. Results and Discussion

3.1. Properties before immersion

All compressive strengths after 56 days of curing were around 60 MPa as the results shown in Table 4. Based on the similar compressive strength, a meaningful comparison of the acid resistance of different sample mixtures was carried out. The results of water absorption, VPV and capillary sorptivity test prior to acid immersion are also shown in Table 4.

Table 4. The compressive strength and porous properties of the mortar samples prior to the exposition to acid solutions.

Sample ID	Compressive strength (MPa)	Water absorption (%)	VPV (%)	Capillary sorptivity ($mm/min^{0.5}$)
80Slag_20FA	57.7	9.2	19.4	0.33
60Slag_40FA	57.7	7.3	17.3	0.17
40Slag_60FA	61.4	6.6	13.3	0.09

In terms of pore-related properties, the largest water absorption, VPV and capillary sorptivity are reported for the 80Slag_20FA mortar followed by the 60Slag_40FA and 40Slag_60FA samples. This

can be attributed to the different amount of water used for mixing the binders in which procedure a higher water/binder ratio usually leads to more pores left after the evaporation of excessive water (Table 2). In terms of porous structures without considering the chemical compositions in different binder matrix, it is reasonable to assume that 80Slag_20FA would have the highest degradation kinetic because the porous properties indicate that more acid solution could get easy ingress into the sample matrix with the largest amount of pores and highest tendency to absorb water via capillary sorptivity [6]. In comparison, it seems that 40Slag_60FA sample should obtain the highest resistance towards acid attacks because it had the smallest porosity, VPV and lowest capillary sorptivity. It is also noteworthy that different alkalinities in different AASF mortar samples because of the different alkali-activator dosages may also influence their performance in acidic environments [23]. However, degradation depth is considered as the only direct method for degradation performance assessment and the influences of all these factors can be reflected on degradation depths.

3.2. Kinetics of degradation over immersion period

Fig. 3 provides an example of the increase in the degradation depth from 28-day to 120-day immersion period for 80Slag_20FA mortar exposed to the phosphoric and sulphuric mixed acid. The degradation depth (mm) as a function of exposure time for all samples is then shown in Fig. 4.

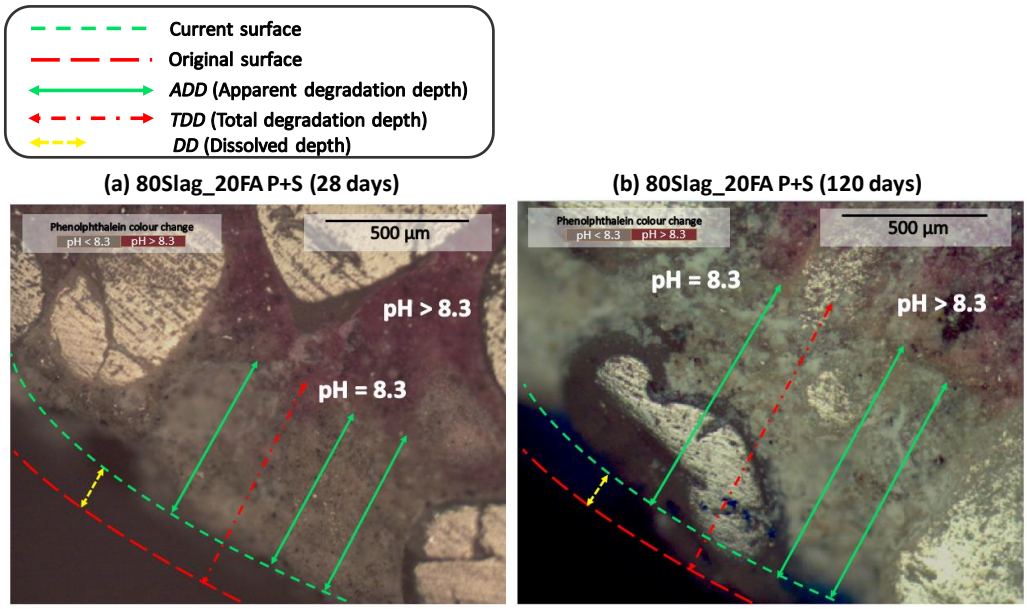


Fig. 3. Optical-microscope measurement results of the sample (80%Slag_20%FA) after being exposed to the phosphoric + sulphuric (simplified as 'P+S' in the Fig. 3) mixed acid for different periods, polished and spayed with phenolphthalein. (a) 28 day-immersion; (b) 120 day-immersion.

A time-dependent degradation depth evolution was obtained for all mixes of the mortar samples regardless of different acid immersion conditions, as shown in Fig. 4(a)-(c). It is found that the *TDD* of all samples after immersion in phosphoric acid for 150 days were greater than those either immersed in the sulphuric acid or the phosphoric and sulphuric mixed acid in this study. In contrast, the samples after the exposure to sulphuric acid had the least *TDD*. The degradation depth of the samples after immersion in the phosphoric and sulphuric mixed acid exhibited an intermediate performance. Therefore, there is no obvious extra effect, such as a synergistic manner proposed by Adam Neville [70], for the phosphoric and sulphuric mixed acid compared to the single acid. The different aggressiveness of the three types of acid solutions can be related to the concentration of hydronium ions H_3O^+ that the acid can release in an aqueous solution depending on acid types and concentrations [71]. In this study, phosphoric and sulphuric acid are both bi-acid in aqueous acid solution (pH < 7) which means that they both can release two hydronium ions in two successive dissociation reactions which are shown below.

In the case of the phosphoric acid, at pH = 2.5, there is two acid functions left (pK_{a1} = 2.12 < pK_{a2} = 7.21 < pK_{a3} = 12.32). The two involved dissociation reactions are as follows:

$$H_3PO_4 + H_2O \rightarrow H_2PO_4^-(aq) + H_3O^+(aq) \text{ (primary)} \quad K_{a1} = 7.5 \times 10^{-3},\ pK_{a1} = 2.12 \tag{1}$$

$$H_2PO_4^- + H_2O \rightarrow HPO_4^{2-}(aq) + H_3O^+(aq) \text{ (secondary)} \quad K_{a2} = 6.2 \times 10^{-8},\ pK_{a2} = 7.21 \tag{2}$$

Therefore, it is apparent that at pH around 2.5 which is slightly higher than 2.12, $H_2PO_4^-$,H_3PO_4 and HPO_4^{2-} coexist in the phosphoric acid solution with the relative fraction of the first one much higher than the other two ions.

For sulphuric acid, there are also two functions left (pK_{a1} very small indicating a very strong acid which completely dissociates in aqueous solutions, pK_{a2} = 1.92) in which case SO_4^{2-} is the main species in the sulphuric acid solution.

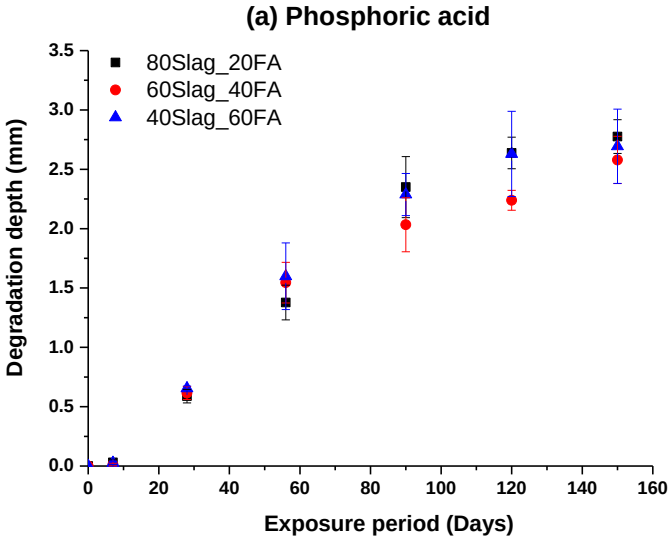
$$H_2SO_4 + H_2O \rightarrow HSO_4^-(aq) + H_3O^+(aq) \text{ (primary)} \quad K_{a1}\ (\text{very large}: 2.4 \times 10^6) \tag{3}$$

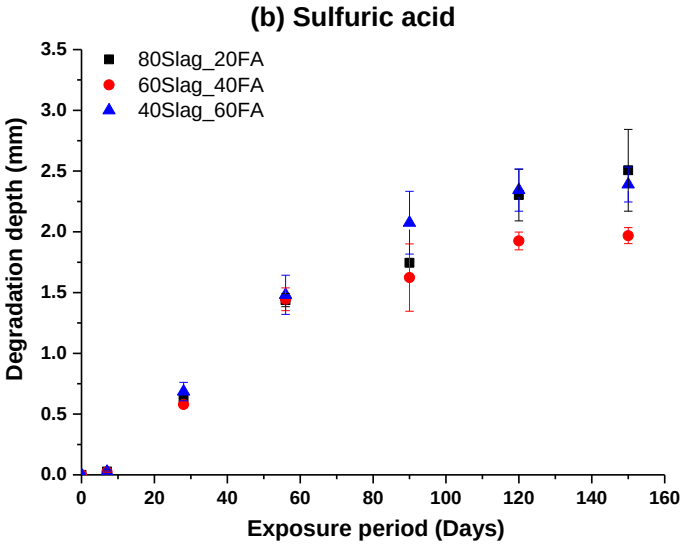
$$HSO_4^- + H_2O \rightarrow SO_4^{2-}(aq) + H_3O^+(aq) \text{ (secondary)} \quad K_{a2} = 1.2 \times 10^{-2},\ pK_{a2} = 1.92 \tag{4}$$

However, due to the partial dissociation of phosphoric acid compared to strong sulphuric acid which dissociates completely in aqueous solution, the concentration of phosphoric acid molecule is higher than that of sulphuric acid with an identical pH [72]. Hence, the amount of hydronium ions that can be

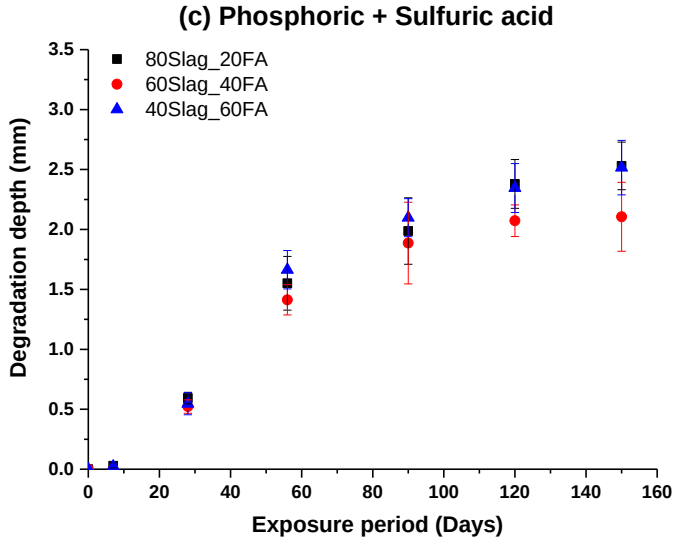
liberated in the phosphoric acid is higher than that of sulphuric acid. This higher concentration of available hydroniums in phosphoric acid solution is possibly responsible for the higher rate of degradation kinetic observed in this study. Similar results were seen in other studies [56, 73] which showed that at the same pH conditions, weak poorly and not-fully dissociated acids would be more aggressive than strong highly dissociated acids towards cementitious materials.

For all acid exposure conditions, 60Slag_40FA seemed to have slightly smaller averaged degradation depths compared to the other formulations (though considering some standard deviations, it could be considered as equivalent to the others). Besides, similar degradation depths were obtained for 80Slag_20FA and 40Slag_60FA samples, especially in the case of the sulphuric acid and the two mixed acid condition. This result indicates that the effect of GGBFS/FA ratios on the relative degradation performance of AAMs is significant, corresponding well with other studies [17, 23]. In addition, it is also noticed that during the initial degradation process (within 7-day immersion period), there was almost no degradation depth measured followed by a significant increase in the degradation depth after 7 days until 56 days. After that, a continuous decreasing rate in the degradation depth development was observed until the end of exposure. This was also reported in another study which confirmed that after a certain period, the degradation rate decreased gradually which might be due to a diffusion-controlled process [21, 46, 51]. Therefore, the whole degradation process of AAMs can be separated into two parts: the first part is from the beginning to about 56-day of immersion (considered as the early stage) and the second stage starts from 56-day until the end of immersion (considered as the later stage).





346



347

348 **Fig. 4. The degradation depths of all mortar samples during 150-day exposure period in the three acid**
349 **environments, (a) phosphoric acid; (b) sulphuric acid and (c) the phosphoric and sulphuric mixed acid.**

350

351 **4. Numerical fitting and long-term predictions of degradation depth**

352 **4.1. Numerical fitting of experimental results**

353 It is possible to divide the degradation process for this study into two stages: an early stage (upto 56
354 days) and a later stage (from 56 days to 150 days).

355 Based on the experimental results within the early stage degradation process, Hill function, as a
356 numerical model was applied to fitting the experimental observations and simulating the early stage of
357 the degradation process. Hill function is used to quantify the degree of cooperative binding between

ligands and a macromolecule such as chondrocyte receptors [74]. It reflects a phenomenon that the response to a specific stimulus may exhibit a threshold behaviour indicating that the response would not take place until the stimuli reach a certain threshold. In this case, the diffusant hydronium ions (H_3O^+) are regarded as a stimulus and the reaction products of AASF binders, e.g. C-A-S-H and/or N-A-S-H can be considered as macromolecules. The Hill function is expressed as the following formula:

$$TDD = \frac{A * t^n}{K^n + t^n} \quad (5)$$

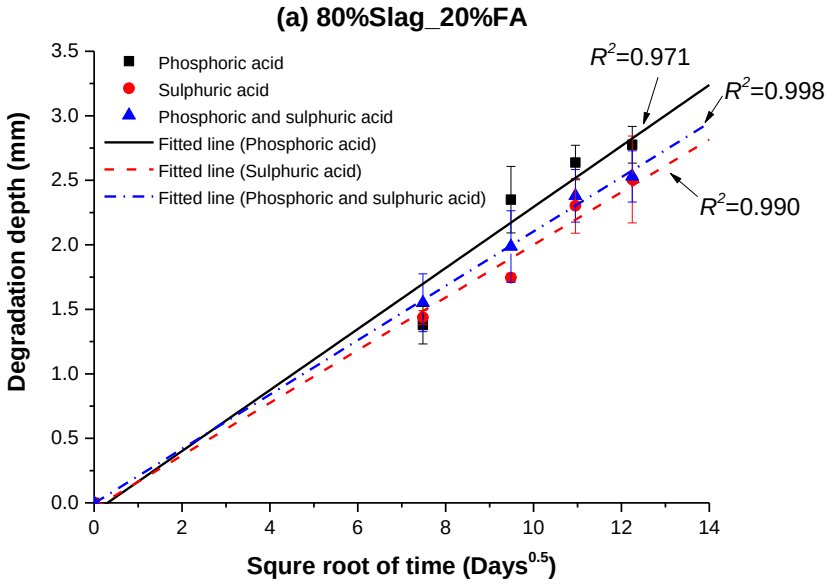
where *A*, *K* and *n* are characteristic values to be determined. '*K*' indicates a certain amount of time during which no obvious degradation process propagates. '*n*' refers to the rate of speed at which degradation reaction proceeds sharply reflected by a significant increase in degradation depths. '*A*' represents the potential capacity of further development of degradation depths. While '*t'* represents the immersion period and *TDD* refers to the total degradation depth. Given the limited number of measurements, the characteristic values '*K*' and '*n*' were fitted using the same value for all samples in the three different acidic environments as the fitted values are very close except '*A*' values. '*A*' values varied significantly depending on different mixtures of the mortars and corresponding acid solutions. Fitted '*A*' values obtained by using non-linear least-square fitting in MatLab are presented in table 6.

In terms of later stage (from 56 days of immersion), a linear fitting of the degradation depth (mm) as a function of square root of time ($Days^{0.5}$) during immersion was first attempted. Fig. 5 (a)-(c) shows the best-fitted lines and the obtained R^2 values are all greater than 0.95 as shown in Table 5, indicating a satisfactory fitting as a diffusion-controlled degradation process [75]. This diffusion-dominated degradation process is also in good agreement with the previous studies showing that the rate of deterioration of some cement-based concrete was proportional to the square root of time [76, 77]. Fick's second law has been widely used to describe the ion transportation caused by diffusion effect because of a concentration gradient between the surrounding aggressive environments and inner part of samples, such as sulphate and chloride migration from outside solutions into concretes [78-81]. During this process, the degradation rate was mainly controlled by the diffusion of ions, such as hydroniums in this case. In the current study, the 56-day of immersion was considered as the starting point of the diffusion-controlled later stage. Hence, only the experimental values from the 56-day immersion were used for further numerical fitting using Fick's second law.

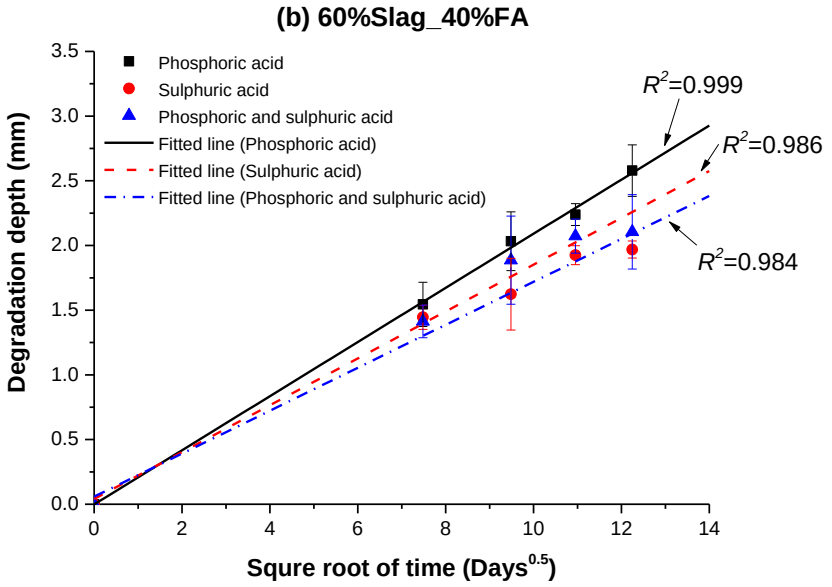
386 Table 5. The fitted coefficient of determination R^2 for the later stage of all mortar samples in the three

387 acid solution environments.

Sample ID	Acid solution types		
	Phosphoric acid	Sulphuric acid	Phosphoric + sulphuric acid
80Slag_20FA	0.971	0.990	0.998
60Slag_40FA	0.999	0.984	0.986
40Slag_60FA	0.989	0.989	0.996



388



389

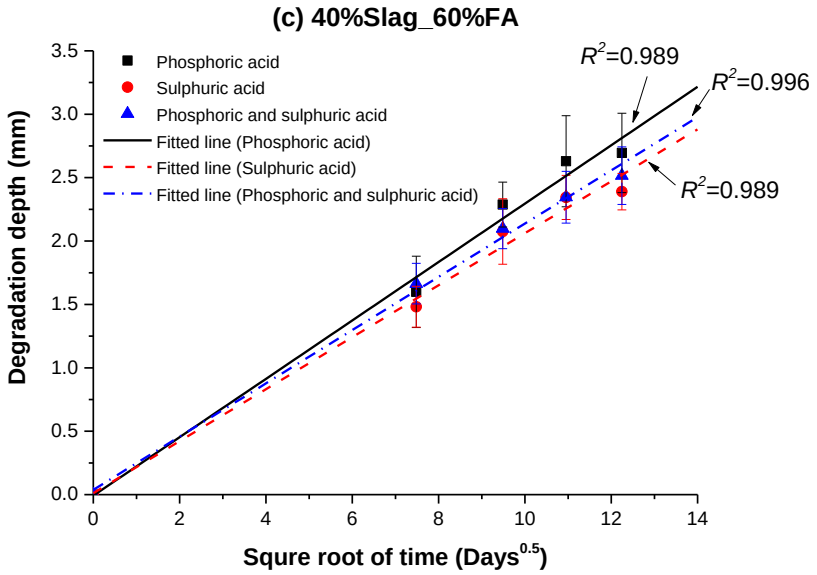


Fig. 5. Degradation depth (mm) evolution as a function of the square root of time (Days$^{0.5}$) for each samples; (a) 80Slag_20FA; (b) 60Slag_40FA; (c) 40Slag_60FA. 'R^2' values represent coefficients of determination. Solid points are the experimental results with error bars indicating one standard deviation either side of the mean value and lines are linearly fitted to showcase the relationship between the degradation depth and square root of exposure time.

According to the Fick's second law, the differential equation for one-dimensional diffusion is as follows:

$$\frac{\partial C(x,t)}{\partial t} = D \cdot \frac{\partial^2 C(x,t)}{\partial x^2} \quad (6)$$

where $C(x,t)$ is the concentration of a specific ion (H_3O^+ in our case) expressed as mol/L, and D is the diffusion coefficient (m^2/s) of the corresponding ion. If the concentration of hydroniums (reflected by the pH value) is assumed to be constant at the surface of the sample, a solution to Fick's second law is as follows:

$$C(x,t) = C_i + (C_s - C_i)\left[1 - erf\left(\frac{x}{2\sqrt{Dt}}\right)\right] \quad (7)$$

where C_i is the initial (or background) concentration of H_3O^+ (mol/L) in the pore solutions of the samples, C_s is the boundary concentration of H_3O^+ (mol/L) at the external surface of the samples. The initial concentration value of H_3O^+ (C_i) in pore solutions of AAMs is in a range between 10^{-12} and 10^{-13} (i.e. a pH ranging from 12 to 13) [22] which is many orders of magnitude less than that of C_s (i.e. $10^{-2.5}$ leading

to a pH of 2.5). Thus, it is reasonable to assume $C_i = 0$ in this study. Then, the time-dependent ion concentration in samples was obtained as:

$$C(x,t)/C_s = \left[1 - erf\left(\frac{x}{2\sqrt{Dt}}\right)\right] \quad (8)$$

where 'erf' is the error function (a special function related to the integral of a normal probability function). As shown in Fig. 2b, the total degradation depth (*TDD*) is the distance between the sample original external boundary and the surface where pH=8.3 (i.e. the colour of phenolphthalein changes from pink or magenta to no colour). Letting C(x, t) = $10^{-8.3}$, Cs = $10^{-2.5}$, the *TDD* can be expressed as,

$$\mathrm{TDD} \approx 6.79\sqrt{D} \cdot \sqrt{t} \quad (9)$$

Based on the different H_3O^+ concentrations at the sample surface, a series of *TDD* can be obtained which are shown below in Eq. (6)-(8). It is worth noting that the apparent diffusion coefficient here is not the real diffusion coefficient of a species (e.g. H_3O^+) in water. Instead, it is a parameter which covers many factors such as acid types, tortuosity and porosity of the binders. It is assumed to be constant for a certain mixture of alkali-activated mortar sample in a specific acid solution regardless of different pH values. The various pH values are assumed to only influence the boundary conditions in the Fick's second law in this study. Changed boundary conditions because of different pH are shown below:

If pH = 1,

$$TDD \approx 7.71\sqrt{D} \cdot \sqrt{t} \quad (10)$$

If pH = 2,

$$TDD \approx 7.11\sqrt{D} \cdot \sqrt{t} \quad (11)$$

If pH = 3,

$$TDD \approx 6.45\sqrt{D} \cdot \sqrt{t} \quad (12)$$

The apparent diffusion coefficients (D) of all samples immersed in three different acidic solutions were obtained by substituting the experimental results into Eq. (9) and using nonlinear least-square best-fit analysis in MATLAB. Diffusion coefficient D has a unit of length/square root of time (*mm/s$^{1/2}$*). The degradation depth is measured in *mm* and the immersion period has a unit of second (*s*). The final obtained diffusion coefficients for all samples in the three acidic solutions are also shown in Table 6.

The successful fitting using the simplified model again confirmed that the degradation depth during later stage process is diffusion-controlled.

Table 6. Numerically fitted apparent diffusion coefficients '*D*' (1×10^{-8} mm^2/s) and '*A*' values (mm) in the Hill function of all samples immersed in the three acid solutions. '*K*' and '*n*' values are '36' and '5' respectively for all samples regardless of different acid solutions and therefore are not listed.

Sample ID	Acid solution types					
	Phosphoric acid		Sulphuric acid		Phosphoric + sulphuric acid	
Parameters	*D*	*A*	*D*	*A*	*D*	*A*
80Slag_20FA	1.32	1.90	1.00	1.65	1.08	1.74
60Slag_40FA	1.04	1.70	0.74	1.42	0.86	1.54
40Slag_60FA	1.32	1.92	1.07	1.72	1.15	1.78

At the beginning of early stage, the degradation process seemed to be delayed, presented as an induction phase. According to the fitting results, all mortar samples regardless of GGBFS/fly ratios and different types of acid solutions had the same duration, expressed as '*K*' = 36 in the Hill function. This indicates that the duration of induction stage is not mainly determined by chemical compositions of AAMs (such as GGBFS/FA ratios and different alkalinities) and acid types. According to Lloyd et al. [46], the early stage of degradation was a chemical-controlled process, which was highly dependent on pH levels of acid solutions. Thus, it is reasonable to assume that the duration of early stage in this study should be similar because all pH values of the acid solutions were kept the same. On the other hand, however, the fitted '*A*' values in Hill functions are different for the three mixtures of mortars in the three acidic media. This indicates that the possible degradation depth at the point of transition from the early stage to later stage differs. In this study, 40Slag_60FA had the greatest '*A*' value indicating the greatest degradation depth at the end of early stage regardless of the acid exposure conditions. However, the lowest capillary sorptivity, water absorption and VPV of 40Slag_60FA imply that it should have the smallest degradation depth without considering the difference in the chemical compositions of all mixture binders. This result is in agreement with another study which revealed that the chemical compositions and components of materials are more predominant than microstructures (i.e. capillary sorptivity or water absorption) for acid resistance [6]. This also points out that less Ca does not necessarily lead to higher resistance with the experimental condition used in this study. More chemical analysis is required in order to explain the results in the future study. Moreover, the sample with greater '*A*' values also exhibits larger diffusion coefficients *D*, suggesting consistent results for the entire degradation process (as shown in Table 6).

Based on the meaning of Hill function, the hindered degradation process at early stage might be attributed to the fact that H_3O^+ are firstly consumed by hydroxyls following the neutralisation reaction: $H_3O^+ + OH^- \rightarrow 2H_2O$. It was already reported that the pH of AASF pore solution is in a range of 13.77-14.76 (depending on alkali-activators used, GGBFS/FA ratios, etc.) which is even higher than that of the pore solution for OPC-based binders (pH > 12) [82]. Therefore, in the initial degradation stage, there are many hydroxyls available in the pore solution to consume H_3O^+ and maintain a high pH level. Thus no obvious degradation depths could be measured at this stage [83, 84]. This mechanism is to some extent analogous to the 'sacrificial medium' effect provided by the high amount of Portlandite ($Ca(OH)_2$) in OPC-based binders. Portlandite plays an important role in 'consuming' most hydroniums with hydroxyls via neutralisation effect when samples were submerged in aggressive acid solutions [9, 85]. In that case, the overall pH level of the pore solutions in OPC-based concrete can remain stable for a certain time.

Furthermore, another possible reason for the absence of degradation depths is that at the very beginning of the acidic attacks, the reaction products precipitated on the surface of the samples and clogged the surface pores. Therefore, the ingress of acid solutions is impeded. At pH between 2.0 and 3.0, the main anion from the phosphoric acid and sulphuric acid solution is supposed to be $H_2PO_4^-$ and SO_4^{2-} respectively. Therefore, the main reaction products due to decalcification process in AAMs is probably monocalcium phosphate $Ca(H_2PO_4)_2$ or $Ca(H_2PO_4)_2 \cdot H_2O$ for phosphoric acid solution and gypsum ($CaSO_4 \cdot 2H_2O$) for sulphuric acid solution with possible chemical reactions:

- Phosphoric acid: $Ca^{2+} + H_2PO_4^- \rightarrow Ca(H_2PO_4)_2$ (calcium dihydrogen phosphate);

  $Ca^{2+} + H_2PO_4^- + H_2O \rightarrow Ca(H_2PO_4)_2 \cdot H_2O$ (calcium dihydrogen phosphate monohydrate)
- Sulphuric acid: $Ca^{2+} + SO_4^{2-} + 2H_2O \rightarrow CaSO_4 \cdot 2H_2O$ (gypsum)

$Ca(H_2PO_4)_2$ and $Ca(H_2PO_4)_2 \cdot H_2O$ both have a solubility of 2.0 g and the water solubility of $CaSO_4 \cdot 2H_2O$ is 0.255 g in 100 ml water (20 ℃). This means that some reaction products are assumed to precipitate on the surface of samples, even clogging surface pores. It can be more obvious when the acid solutions are calcium-saturated before each renewal. This is evidenced by some white compounds detectable on the surface of the samples after 56-day immersion period when the sample was naturally dried under the ambient environment (Fig. 6). This is in consistent with the case reported by J. Shen et al. [86] that in some extreme conditions, the surface pores could be clogged because of the formations of some reaction products. Hence, during the reaction-controlled early stage, it is probably the clogging

491 effect caused by the reaction products that led to a delayed degradation evolution in the early stage.
492 This result is also consistent with the finding in the study that sulphuric acid-induced attack mainly
493 occurs at the sample surfaces if there is no flow of fluid with the formation of gypsums (molar volume:
494 73.84 cm^3/mol) on the sample surface when the surrounding pH is at 2.0 [58]. A study also has reported
495 a reaction-controlled degradation process in the early stage of exposition for AAMs [46]. However, as
496 specific reaction mechanisms are not fully explained, especially for AAMs in phosphoric acid solutions,
497 more research is therefore necessary. The accumulation of the precipitated reaction products on the
498 surface might be another factor that results in the transition from early stage to later stage as
499 hydroniums had to diffuse through this product layer first before entering the sample matrix.



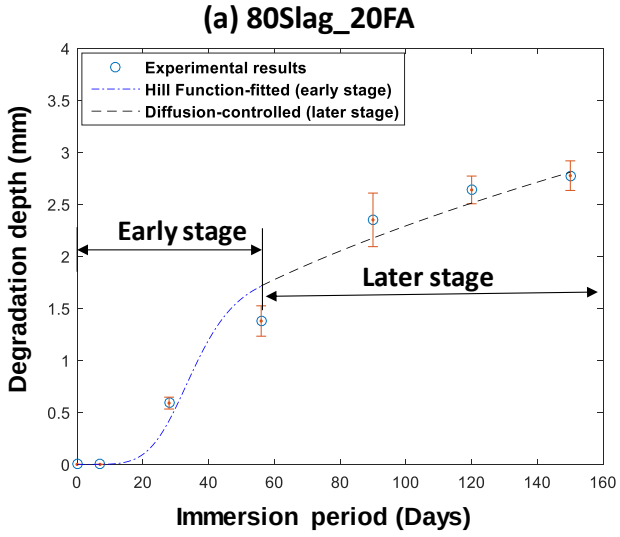
500

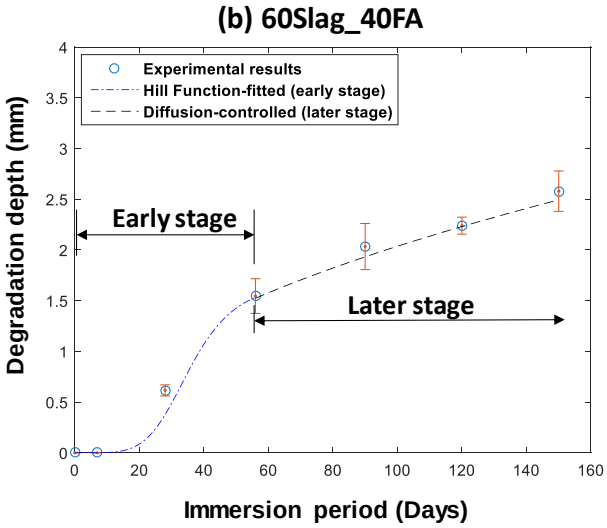
501 **Fig. 6. The white reaction products precipitated on the sample surface clogging the surface pores after 56-day**
502 **immersion period (The picture was taken after the sample was taken out from the acid solution and dried**
503 **under ambient condition for upto 3 hours).**

504 In terms of later stage fitted by using Fick's second law with the diffusion coefficients shown in Table
505 6, it is evident that the 60%Slag_40%FA sample had the lowest diffusion coefficient (1.04×10^{-8} mm^2/s)
506 in phosphoric acid solution. On the other hand, the 40%Slag_60%FA and 80%Slag_20%FA sample
507 had a similar highest diffusion coefficient at around 1.32×10^{-8} mm^2/s. In the sulphuric and the
508 phosphoric and sulphuric mixed acid, 60%Slag_40%FA sample also had the least diffusion coefficient,
509 0.74×10^{-8} mm^2/s and 0.86×10^{-8} mm^2/s respectively. While the sample 40%Slag_60%FA had the
510 greatest diffusion coefficient, respectively 1.07×10^{-8} mm^2/s and 1.15×10^{-8} mm^2/s in the sulphuric and
511 the phosphoric and sulphuric mixed acid. Apparently, the 60%Slag_40%FA sample performed the best
512 with the lowest diffusion coefficient compared to the other sample mixtures in all acid solutions. The

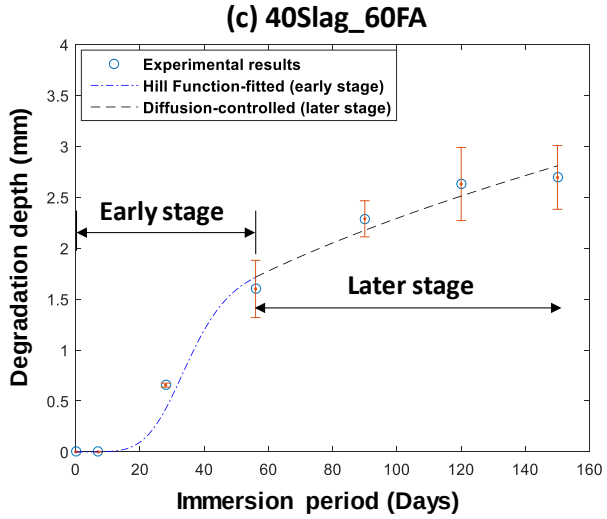
40%Slag_60%FA sample, which exhibited the greatest degradation depth, had the largest diffusion coefficient accordingly among the tested samples in all solutions. The diffusion-controlled later stage can be due to the mechanically stable degraded layer which is less soluble. It is known as a residue gel rich in Si and Al which can act as a protection layer, hence limiting further ingress of hydroniums [87]. Besides, it can also be partially ascribed to the precipitations of reaction products such as calcium salts which is already discussed in the early stage part.

Fig. 7-9 show the overall degradation process including the two stages to compare the degradation process for various mixtures of samples in different acid solutions. To conclude, the observed degradation process in this study can be separated into two major stages including the early stage and later stage. In the early stage, the empirical Hill function was applied to fitting the experimental data which showed that at the very beginning of the degradation, there was almost no degradation depths for at least several days. Then there was an obvious degradation depth (approximately 0.5 mm) after 28-day exposure to acid solutions which indicates a significant increase in degradation rate. The highest increasing rate of the degradation depth occurred at around 36 days of immersion, corresponding to the parameter '*K*' = 36 in Hill function for all samples in the three different acid media. This value can be regarded as a turning point after which the degradation process gradually converted into the later stage. In the later stage, the degradation process was diffusion-controlled showing a linear increment in degradation depths as a function of square root of immersion period (Fig. 5). The growth in degradation depths in this stage was apparently limited, likely due to the existence of mechanically sound degraded layer and formation of newly-formed reaction products in the degraded layer which hindered further penetrations of hydronium ions [46].





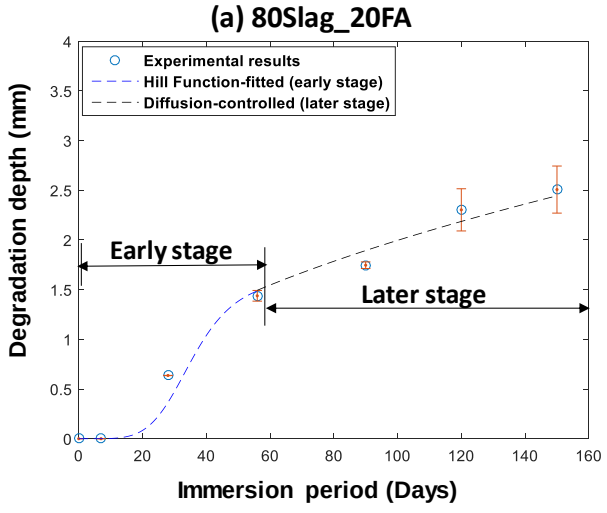
535



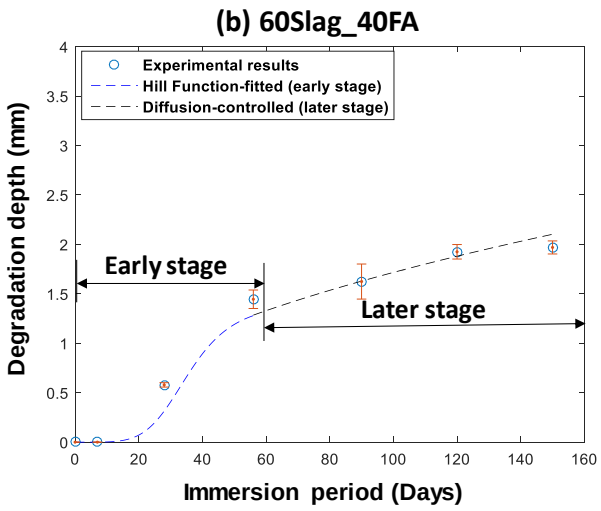
536

537 **Fig. 7. Time-dependent degradation depths of different samples in the phosphoric acid during the immersion**

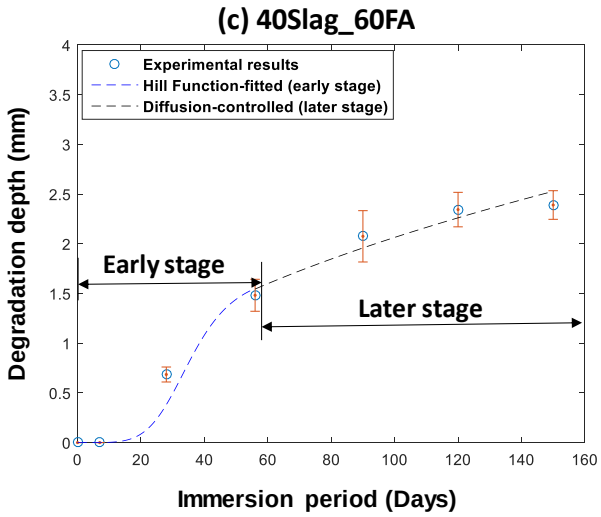
538 **period. (a) 80Slag_20FA; (b) 60Slag_40FA; (c) 40Slag_60FA.**



539



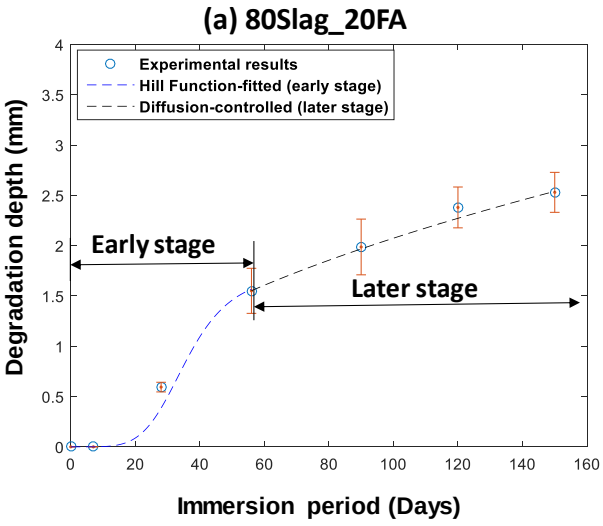
540



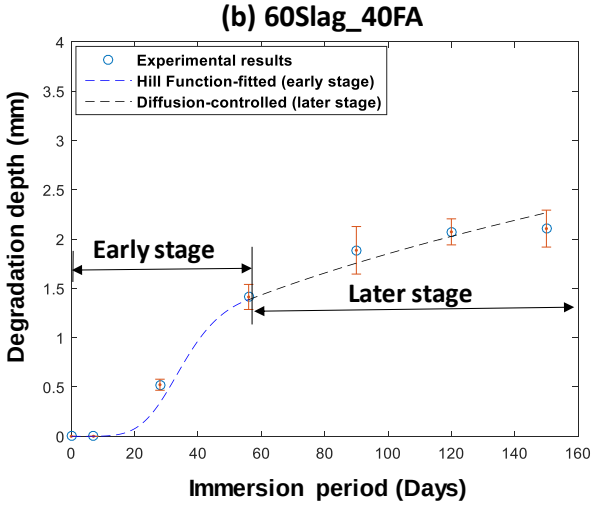
541

542 **Fig. 8. Time-dependent degradation depths of different samples in the sulphuric acid during the immersion**

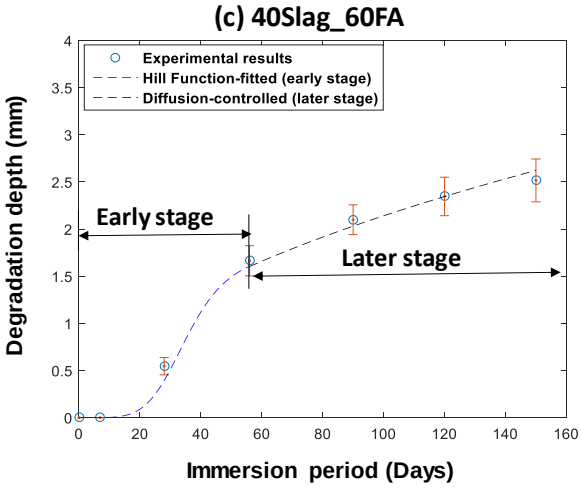
543 **period. (a) 80Slag_20FA; (b) 60Slag_40FA; (c) 40Slag_60FA.**



544



545



546

547 **Fig. 9. Time-dependent degradation depths of different samples in the phosphoric and sulphuric mixed acid**

548 **during the immersion periods. (a) 80Slag_20FA; (b) 60Slag_40FA; (c) 40Slag_60FA.**

When comparing the different samples, the peculiarities of the microstructures and compositions of the AASF mortars in the study can be responsible for their different acid resistance capabilities [88, 89]. In the study, the 80%Slag_20%FA sample had the highest initial VPV and water absorption as well as water sorptivity (Table 4). The sorptivity can reveal the transport mechanisms of acid solutions in the mortar samples [6]. Combined with higher VPV and water absorption, greater sorptivity suggests a porous structure with a high connectivity and many finer interconnected voids. All of these lead to a much easier ingress of acid solutions and aggressive ions into the matrix binders compared to other mixtures of mortars. Thus, within a certain period, far more hydronium ions with water flowed into the samples which explained why the 80%Slag_20%FA had a relatively larger degradation depth. On the other hand, the 40%Slag_60%FA sample had a denser porous structure with lower VPV, water absorption and water sorptivity. According to N.K. Lee et al. [89], an increase in fly ash content leads to more sodium aluminosilicate hydrate (N-A-S-H) gel and less C-A-S-H, and the former one is less dense compared to the latter. Therefore, the sample with a higher amount of fly ash replacing slag contains more N-A-S-H, developing a more porous matrix which reduced the resistance towards ion transport [44]. Therefore, H_3O^+ attacked the bulk matrix of the samples easier which was responsible for the greater degradation depth compared to the other mixtures of the samples. The 60%Slag_40%FA sample seemed to overcome the disadvantages of the other two peers and made a great compromise between the pore networks and the geopolymerisation products. It has a certain amount of calcium which results in the formation of a denser C-A-S-H type gel along with a relatively compact porous microstructure.

4.2. Predictions of long-term performance between AAMs and OPC based mortars

Yuan et al. [51] carried out an experiment and conducted long-term simulation based on Kawai's [58] 90-day experiments where OPC-based mortars (w/b: 0.35 and initial compressive strength cured after 28 days was 47.2 MPa) were subjected to sulphuric acid attack with a pH at 2.0 for 24 months. Then a generally believed relationship between the degradation depth and exposure time was used to model the degradation process (Method 1 as discussed in the Kawai's study [58]) [21]. The relationship is almost the same as the simplified model for later-stage degradation which also highlights a linear increase in degradation depth of concrete due to acid attacks including sulphuric acid against the square root of time as follows:

$$TDD = b \cdot \sqrt{t} \quad (13)$$

where, *TDD* is the total degradation depth (mm) as described before, *t* represents the exposure time (month) in acidic solution and *b* is a constant. This equation indicates that the degradation kinetic is controlled by the diffusion rate of acid under the assumption that degradation products remain on the surface [51]. Since the samples in this study were also statically subjected to acidic attacks without shearing forces from splashing or running water, the particles were also assumed to precipitate and remain on the surface. Based on Eq. (13), Yuan et al.[51] calculated the value of constant *b* which is 2.5 mm/month$^{1/2}$ and the degradation depth of this OPC-based mortar was then predicted. After 50-year immersion, it is estimated that the degradation depth can be as much as 61.24 mm.

As the alkali-activated mortar samples in this study were also immersed in sulphuric acid with a similar pH condition (pH = 2.5 ± 0.5), the corresponding derived diffusion coefficients for each sample mixture are assumed to be constant. The only difference is the boundary condition which changes into Eq. (11). Then Eq. (11) and derived diffusion coefficients for sulphuric acid immersion were used to predict the degradation depths after 50-year immersion period. The predicted numerical results are compared to that of OPC-based mortars mentioned before, as shown in Fig. 10. After 50-year exposure, the increasing order of degradation depths are 60%Slag_40%FA, 80%Slag_20%FA and 40%Slag_60%FA with the degradation depth at 24.29, 28.23 and 29.20 mm respectively. Apparently, the degradation depths of all alkali-activated mortars are much less than that of the OPC-based mortar sample. As a result, the degradation depth can be decreased by around 60.3%, 53.9% and 52.3% if the OPC-based tested samples are replaced by 60%Slag_40%FA, 80%Slag_20%FA and 40%Slag_60%FA respectively in this study.

It is worth noting that the 56-day compressive strength of the AASF mortar samples in this study was higher than the 47.2 MPa compressive strength after 28 days of curing in Kawai's study [58]. Considering the continuous cement hydration, the 56-day compressive strength for this OPC mortar should be higher and it is speculated to be around 55.6 MPa according to a formula proposed by Liu et al. [90]. Therefore a reasonable comparison was carried out above. However, it still has to be admitted that the compressive strength difference between the AASF mortars (ranging between 57.7 and 61.4 MPa) in this study and the OPC-based counterpart in Kawai's study [58] (55.6 MPa as speculated) is possibly another reason for the less degradation depth of the former ones as compared to the latter since a higher compressive strength usually indicates a denser microstructure. Therefore, further

research with regards to a systematic comparison between the AASF and OPC-based mortars should be conducted.

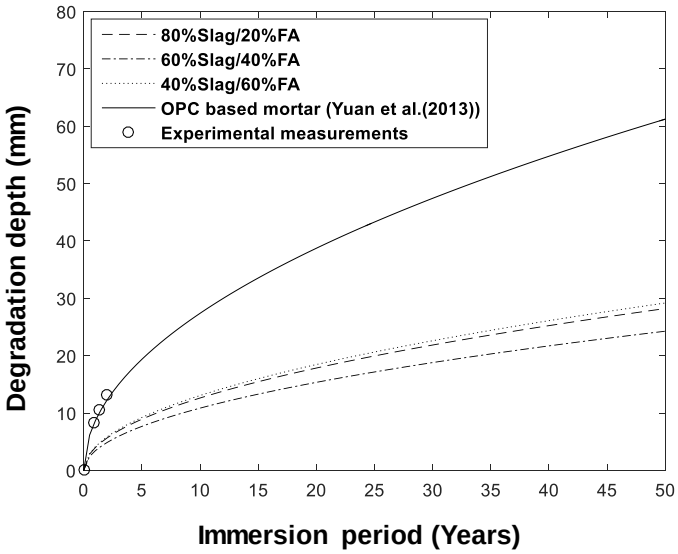


Fig. 10. The comparison between the numerical predictions based on the present study and the experimental results as well as corresponding simulation equations derived from Yuan et al. (2013).

Limitations

It should be mentioned that this study mainly focused on the degradation of mortar specimens instead of concrete which is a composite material composed of fine and coarse aggregates bonded together with cement. In addition, our theoretical analysis ignored the possible changes in diffusion coefficient of ions due to the damages of mortar microstructures with degradation progression. Our future will focus on the degradation of concrete under acid conditions which might provide more representative results and the chemical processes involved in the early stage of degradation will also be explored.

5. Conclusions

The present study investigated experimentally the degradation depth evolution of AASF mortars under three aggressive acid solutions. The following conclusions can be summarised:

- Among all the three types of acids with similar pH values: phosphoric acid, sulphuric acid and the mixture of phosphoric acid and sulphuric acid, phosphoric acid caused the most severe degradation to AASF mortars due to its largest amount of available hydroniums;
- The AASF mortar with a slag/fly ash ratio at 60:40 displayed the best durability performance after immersion in the three types of acids for 150 days probably due to its higher amount of C-

A-S-H (compared to 40%Slag_60%FA) and a relatively more densified structure (compared to 80%Slag_20%FA);

- The degradation of AASF mortars can be divided into two stages: (1) Early stage - a chemical dominated process which can be described by using Hill function; and (2) Later stage - a diffusion dominated process which is described by using Fick's second law.
- Theoretical prediction shows that the reduction in the degradation depth of AASF mortars after 50 years' immersion in sulphuric acid (pH=2.0) could be in a range between 52% - 60% compared to that of the OPC-based mortar.

Acknowledgement

This work was supported by Chinese Scholarship Council (CSC), the Australian Research Council (IH150100006), the Geopolymer and Minerals Processing Group laboratory at The University of Melbourne. The authors also express their thanks Mrs. Laura Jukes for her assistance with the experimental work.

Reference

1. Parande, A., P. Ramsamy, S. Ethirajan, C. Rao, and N. Palanisamy. *Deterioration of reinforced concrete in sewer environments*. in *Proceedings of the Institution of Civil Engineers-Municipal Engineer*. 2006. Thomas Telford Ltd.
2. Gutberlet, T., H. Hilbig, and R. Beddoe, *Acid attack on hydrated cement—Effect of mineral acids on the degradation process.* Cement and Concrete Research, 2015. **74**: p. 35-43.
3. Bakharev, T., J.G. Sanjayan, and Y.B. Cheng, *Resistance of alkali-activated slag concrete to acid attack.* Cement and Concrete Research, 2003. **33**(10): p. 1607-1611.
4. Kaid, N., M. Cyr, S. Julien, and H. Khelafi, *Durability of concrete containing a natural pozzolan as defined by a performance-based approach.* Construction and Building Materials, 2009. **23**(12): p. 3457-3467.
5. Siad, H., H.A. Mesbah, H. Khelafi, S. Kamali-Bernard, and M. Mouli, *Effect of mineral admixture on resistance to sulphuric and hydrochloric acid attacks in self-compacting concrete.* Canadian journal of civil engineering, 2010. **37**(3): p. 441-449.
6. Albitar, M., M.M. Ali, P. Visintin, and M. Drechsler, *Durability evaluation of geopolymer and conventional concretes.* Construction and Building Materials, 2017. **136**: p. 374-385.
7. Oueslati, O. and J. Duchesne, *Resistance of blended cement pastes subjected to organic acids: Quantification of anhydrous and hydrated phases.* Cement and Concrete Composites, 2014. **45**: p. 89-101.
8. Gutiérrez-Padilla, M.G.D., A. Bielefeldt, S. Ovtchinnikov, M. Hernandez, and J. Silverstein, *Biogenic sulfuric acid attack on different types of commercially produced concrete sewer pipes.* Cement and Concrete Research, 2010. **40**(2): p. 293-301.
9. O'Connell, M., C. McNally, and M.G. Richardson, *Biochemical attack on concrete in wastewater applications: A state of the art review.* Cement and Concrete Composites, 2010. **32**(7): p. 479-485.
10. Monteny, J., E. Vincke, A. Beeldens, N. De Belie, L. Taerwe, D. Van Gemert, and W. Verstraete, *Chemical, microbiological, and in situ test methods for biogenic sulfuric acid corrosion of concrete.* Cement and Concrete Research, 2000. **30**(4): p. 623-634.

11. Huber, B., H. Hilbig, M.M. Mago, J.E. Drewes, and E. Müller, *Comparative analysis of biogenic and chemical sulfuric acid attack on hardened cement paste using laser ablation-ICP-MS.* Cement and Concrete Research, 2016. **87**: p. 14-21.
12. Fattuhi, N. and B. Hughes, *The performance of cement paste and concrete subjected to sulphuric acid attack.* Cement and Concrete Research, 1988. **18**(4): p. 545-553.
13. Vincke, E., S. Verstichel, J. Monteny, and W. Verstraete, *A new test procedure for biogenic sulfuric acid corrosion of concrete.* Biodegradation. **10**(6): p. 421-428.
14. De Belie, N., J. Monteny, A. Beeldens, E. Vincke, D. Van Gemert, and W. Verstraete, *Experimental research and prediction of the effect of chemical and biogenic sulfuric acid on different types of commercially produced concrete sewer pipes.* Cement and Concrete Research, 2004. **34**(12): p. 2223-2236.
15. De-Bashan, L.E. and Y. Bashan, *Recent advances in removing phosphorus from wastewater and its future use as fertilizer (1997–2003).* Water research, 2004. **38**(19): p. 4222-4246.
16. Xiaowei Zhang, J.H., Zhihai Hao, Zhonghan Chen, *Comparative study on corrosion of two Kinds of Acids to Concrete.* CHINA CONCRETE AND CEMENT PRODUCTS, 2003(05): p. 08-12.
17. Aiken, T.A., W. Sha, J. Kwasny, and M.N. Soutsos, *Resistance of geopolymer and Portland cement based systems to silage effluent attack.* Cement and Concrete Research, 2017. **92**: p. 56-65.
18. Allahverdi, A. and F. Skvara, *Nitric acid attack on hardened paste of geopolymeric cements, Part 2.* CERAMICS SILIKATY, 2001. **45**: p. 143-150.
19. Allahverdi, A. and F. Skvara, *Nitric acid attack on hardened paste of geopolymeric cements, Part 1.* CERAMICS SILIKATY, 2001. **45**: p. 81-88.
20. Pavlik, V., *Corrosion of hardened cement paste by acetic and nitric acids Part III: Influence of water/cement ratio.* Cement and Concrete Research, 1996. **26**(3): p. 475-490.
21. Pavlik, V., *Corrosion of hardened cement paste by acetic and nitric acids part I: Calculation of corrosion depth.* Cement and concrete research, 1994. **24**(3): p. 551-562.
22. Sand, W. and E. Bock, *Biodeterioration of mineral materials by microorganisms—biogenic sulfuric and nitric acid corrosion of concrete and natural stone.* Geomicrobiology Journal, 1991. **9**(2-3): p. 129-138.
23. Aiken, T.A., J. Kwasny, W. Sha, and M.N. Soutsos, *Effect of slag content and activator dosage on the resistance of fly ash geopolymer binders to sulfuric acid attack.* Cement and Concrete Research, 2018. **111**: p. 23-40.
24. Mehta, A. and R. Siddique, *Sulfuric acid resistance of fly ash based geopolymer concrete.* Construction and Building Materials, 2017. **146**: p. 136-143.
25. Provis, J.L., A. Palomo, and C. Shi, *Advances in understanding alkali-activated materials.* Cement and Concrete Research, 2015. **78, Part A**: p. 110-125.
26. Flanigen, E.M., J. Jansen, and H. van Bekkum, *Introduction to zeolite science and practice*. Vol. 58. 1991: Elsevier.
27. Temuujin, J.v., A. Van Riessen, and R. Williams, *Influence of calcium compounds on the mechanical properties of fly ash geopolymer pastes.* Journal of hazardous materials, 2009. **167**(1): p. 82-88.
28. Pacheco-Torgal, F., J. Castro-Gomes, and S. Jalali, *Alkali-activated binders: A review: Part 1. Historical background, terminology, reaction mechanisms and hydration products.* Construction and Building Materials, 2008. **22**(7): p. 1305-1314.
29. Davidovits, J., D.C. Comrie, J.H. Paterson, and D.J. Ritcey, *Geopolymeric concretes for environmental protection.* Concrete International, 1990. **12**(7): p. 30-40.
30. Ukrainczyk, N.M., M.; Vogt, O.; Koenders, E, *Geopolymer, Calcium Aluminate, and Portland Cement-Based Mortars: Comparing Degradation Using Acetic Acid.* materials, 2019. **12**.
31. Bernal, S.A., R.M. de Gutiérrez, and J.L. Provis, *Engineering and durability properties of concretes based on alkali-activated granulated blast furnace slag/metakaolin blends.* Construction and Building Materials, 2012. **33**: p. 99-108.

32. Provis, J.L., C.Z. Yong, P. Duxson, and J.S. van Deventer, *Correlating mechanical and thermal properties of sodium silicate-fly ash geopolymers.* Colloids and Surfaces A: Physicochemical and Engineering Aspects, 2009. **336**(1): p. 57-63.
33. Bakharev, T., J. Sanjayan, and Y.-B. Cheng, *Resistance of alkali-activated slag concrete to acid attack.* Cement and Concrete Research, 2003. **33**(10): p. 1607-1611.
34. Li, Zihui, Peethamparan, and Sulapha, *Leaching resistance of alkali-activated slag and fly ash mortars exposed to organic acid.*
35. Davidovits, J., *Geopolymer, Green Chemistry and Sustainable Development Solutions: Proceedings of the World Congress Geopolymer 2005*. 2005: Geopolymer Institute.
36. Fernández-Jiménez, A., I. Garcia-Lodeiro, and A. Palomo, *Durability of alkali-activated fly ash cementitious materials.* Journal of Materials Science, 2007. **42**(9): p. 3055-3065.
37. Varga, C., M. Alonso, R.M. De Gutierrez, J. Mejía, and F. Puertas, *Decalcification of alkali-activated slag pastes. Effect of the chemical composition of the slag.* Materials and Structures, 2015. **48**(3): p. 541-555.
38. Van Deventer, J.S., J.L. Provis, P. Duxson, and D.G. Brice, *Chemical research and climate change as drivers in the commercial adoption of alkali activated materials.* Waste and Biomass Valorization, 2010. **1**(1): p. 145-155.
39. Lloyd, R.R., J.L. Provis, and J.S. Van Deventer, *Pore solution composition and alkali diffusion in inorganic polymer cement.* Cement and Concrete Research, 2010. **40**(9): p. 1386-1392.
40. Li, Z. and S. Liu, *Influence of slag as additive on compressive strength of fly ash-based geopolymer.* Journal of Materials in civil engineering, 2007. **19**(6): p. 470-474.
41. Puertas, F., S. Martínez-Ramírez, S. Alonso, and T. Vazquez, *Alkali-activated fly ash/slag cements: strength behaviour and hydration products.* Cement and concrete research, 2000. **30**(10): p. 1625-1632.
42. Goretta, K., N. Chen, F. Gutierrez-Mora, J. Routbort, G. Lukey, and J. Van Deventer, *Solid-particle erosion of a geopolymer containing fly ash and blast-furnace slag.* Wear, 2004. **256**(7-8): p. 714-719.
43. Ling, Y., K. Wang, W. Li, G. Shi, and P. Lu, *Effect of slag on the mechanical properties and bond strength of fly ash-based engineered geopolymer composites.* Composites Part B: Engineering, 2019. **164**: p. 747-757.
44. Ismail, I., S.A. Bernal, J.L. Provis, R. San Nicolas, D.G. Brice, A.R. Kilcullen, S. Hamdan, and J.S. van Deventer, *Influence of fly ash on the water and chloride permeability of alkali-activated slag mortars and concretes.* Construction and Building Materials, 2013. **48**: p. 1187-1201.
45. Ismail, I., S.A. Bernal, J.L. Provis, R. San Nicolas, S. Hamdan, and J.S.J. van Deventer, *Modification of phase evolution in alkali-activated blast furnace slag by the incorporation of fly ash.* Cement and Concrete Composites, 2014. **45**: p. 125-135.
46. Lloyd, R.R., J.L. Provis, and J.S. van Deventer, *Acid resistance of inorganic polymer binders. 1. Corrosion rate.* Materials and structures, 2012. **45**(1-2): p. 1-14.
47. Provis, J.L., R.J. Myers, C.E. White, V. Rose, and J.S. van Deventer, *X-ray microtomography shows pore structure and tortuosity in alkali-activated binders.* Cement and Concrete Research, 2012. **42**(6): p. 855-864.
48. Bernal, S.A., V. Bílek, M. Criado, A. Fernández-Jiménez, E. Kavalerova, P.V. Krivenko, M. Palacios, A. Palomo, J.L. Provis, and F. Puertas, *Durability and testing–degradation via mass transport*, in *Alkali Activated Materials*. 2014, Springer. p. 223-276.
49. Bernal, S.A. and J.L. Provis, *Durability of Alkali‐Activated Materials: Progress and Perspectives.* Journal of the American Ceramic Society, 2014. **97**(4): p. 997-1008.
50. Ariffin, M., M. Bhutta, M. Hussin, M.M. Tahir, and N. Aziah, *Sulfuric acid resistance of blended ash geopolymer concrete.* Construction and Building Materials, 2013. **43**: p. 80-86.
51. Yuan, H., P. Dangla, P. Chatellier, and T. Chaussadent, *Degradation modelling of concrete submitted to sulfuric acid attack.* Cement and Concrete Research, 2013. **53**: p. 267-277.

52. Bertron, A., J. Duchesne, and G. Escadeillas, *Degradation of cement pastes by organic acids.* Materials and structures, 2007. **40**(3): p. 341-354.
53. Bertron, A., J. Duchesne, and G. Escadeillas, *Accelerated tests of hardened cement pastes alteration by organic acids: analysis of the pH effect.* Cement and Concrete Research, 2005. **35**(1): p. 155-166.
54. Larreur-Cayol, S., A. Bertron, and G. Escadeillas, *Degradation of cement-based materials by various organic acids in agro-industrial waste-waters.* Cement and Concrete Research, 2011. **41**(8): p. 882-892.
55. Huber, B., H. Hilbig, J.E. Drewes, and E. Müller, *Evaluation of concrete corrosion after short- and long-term exposure to chemically and microbially generated sulfuric acid.* Cement and Concrete Research, 2017. **94**: p. 36-48.
56. Shi, C. and J. Stegemann, *Acid corrosion resistance of different cementing materials.* Cement and Concrete Research, 2000. **30**(5): p. 803-808.
57. Shi, C., *Corrosion resistance of alkali-activated slag cement.* Advances in cement research, 2003. **15**(2): p. 77-81.
58. Kawai, K., S. Yamaji, and T. Shinmi. *Concrete deterioration caused by sulfuric acid attack*. in *International Conference on Durability of Building Materials and Components. LYON [France]*. 2005.
59. Xiao, J., W. Qu, W. Li, and P. Zhu, *Investigation on effect of aggregate on three non-destructive testing properties of concrete subjected to sulfuric acid attack.* Construction and Building Materials, 2016. **115**: p. 486-495.
60. Levenspiel, O., *Chemical reaction engineering.* Industrial & engineering chemistry research, 1999. **38**(11): p. 4140-4143.
61. Jie Ren, L.Z., Rackel San Nicolas, *Degradation process of alkali-activated slag/fly ash and Portland cement-based pastes exposed to phosphoric acid.* Construction and Building Materials, 2019.
62. Ren, J., S.-Y. Guo, J. Su, T.-J. Zhao, J.-Z. Chen, and S.-L. Zhang, *A novel TiO2/Epoxy resin composited geopolymer with great durability in wetting-drying and phosphoric acid solution.* Journal of Cleaner Production, 2019.
63. Ismail, I., S.A. Bernal, J.L. Provis, R. San Nicolas, S. Hamdan, and J.S. van Deventer, *Modification of phase evolution in alkali-activated blast furnace slag by the incorporation of fly ash.* Cement and Concrete Composites, 2014. **45**: p. 125-135.
64. Satoh, H., M. Odagiri, T. Ito, and S. Okabe, *Microbial community structures and in situ sulfate-reducing and sulfur-oxidizing activities in biofilms developed on mortar specimens in a corroded sewer system.* Water research, 2009. **43**(18): p. 4729-4739.
65. Bertron, A., S. Larreur-Cayol, T.M.T. Le, and G. Escadeillas, *Degradation of cementitious materials by some organic acids found in agroindustrial effluents.* Proceedings of the RILEM TC, 2009: p. 96-107.
66. ASTM, A., *C109/C109M-Standard Test Method for Compressive Strength of Hydraulic Cement Mortars (Using 2-in. or (50-mm) Cube Specimens); 2013. 2.* Scope of work shall include but not be limited to the following:-Suspended metal grid for acoustical tile ceiling system, 1999.
67. ASTM, C., *642, Standard test method for density, absorption, and voids in hardened concrete.* Annual book of ASTM standards, 2006. **4**.
68. Astm, C., *1585-04. Standard test method for measurement of rate of absorption of water by hydraulic-cement concretes.* ASTM International, 2004.
69. Ismail, I., S.A. Bernal, J.L. Provis, S. Hamdan, and J.S. van Deventer, *Drying-induced changes in the structure of alkali-activated pastes.* Journal of Materials Science, 2013. **48**(9): p. 3566-3577.
70. Neville, A., *Consideration of durability of concrete structures: Past, present, and future.* Materials and structures, 2001. **34**(2): p. 114-118.

71. Alexander, M. and C. Fourie, *Performance of sewer pipe concrete mixtures with portland and calcium aluminate cements subject to mineral and biogenic acid attack.* Materials and structures, 2011. **44**(1): p. 313-330.
72. Koenig, A. and F. Dehn, *Main considerations for the determination and evaluation of the acid resistance of cementitious materials.* Materials and Structures, 2016. **49**(5): p. 1693-1703.
73. Beddoe, R.E. and H.W. Dorner, *Modelling acid attack on concrete: Part I. The essential mechanisms.* Cement and Concrete Research, 2005. **35**(12): p. 2333-2339.
74. Zhang, L., B.S. Gardiner, D.W. Smith, P. Pivonka, and A.J. Grodzinsky, *Integrated model of IGF-I mediated biosynthesis in a deformed articular cartilage.* Journal of Engineering Mechanics, 2009. **135**(5): p. 439-449.
75. Matteo, E.N. and G.W. Scherer, *Experimental study of the diffusion-controlled acid degradation of Class H Portland cement.* International Journal of Greenhouse Gas Control, 2012. **7**: p. 181-191.
76. Zongjin, L., C. Leung, and Y. Xi, *Structural Renovation in Concrete.* Book Published by Spon Press an imprint of Taylor & Francis, London and New York, 2009.
77. Code, M., *International Federation for Structural Concrete (fib).* Federal Institute of Technology Lausanne–EPFL, Section Génie Civil, Swizerland, 2010: p. 978-3.
78. Zuo, X.-B., W. Sun, and C. Yu, *Numerical investigation on expansive volume strain in concrete subjected to sulfate attack.* Construction and Building Materials, 2012. **36**: p. 404-410.
79. Sun, C., J. Chen, J. Zhu, M. Zhang, and J. Ye, *A new diffusion model of sulfate ions in concrete.* Construction and Building Materials, 2013. **39**: p. 39-45.
80. Zhu, X., G. Zi, Z. Cao, and X. Cheng, *Combined effect of carbonation and chloride ingress in concrete.* Construction and Building Materials, 2016. **110**: p. 369-380.
81. Frederiksen, J.M., L. Mejlbro, and L.-O. Nilsson, *Fick's 2 nd law-Complete solutions for chloride ingress into concrete.* Report TVBM-3146, Lund Institute of Technology, Sweden, 2008.
82. Zuo, Y., M. Nedeljković, and G. Ye, *Pore solution composition of alkali-activated slag/fly ash pastes.* Cement and Concrete Research, 2019. **115**: p. 230-250.
83. Abdel-Gawwad, H. and S.A. El-Aleem, *Effect of reactive magnesium oxide on properties of alkali activated slag geopolymer cement pastes.* Ceramics–Silikáty, 2015. **59**(1): p. 37-47.
84. Song, X., M. Marosszeky, M. Brungs, and R. Munn. *Durability of fly ash based geopolymer concrete against sulphuric acid attack*. in *International Conference on Durability of Building Materials And Components, Lyon [France]*. 2005.
85. Gutberlet, T., H. Hilbig, and R.E. Beddoe, *Acid attack on hydrated cement — Effect of mineral acids on the degradation process.* Cement and Concrete Research, 2015. **74**: p. 35-43.
86. Shen, J., P. Dangla, and M. Thiery, *Reactive transport modeling of CO 2 through cementitious materials under CO 2 geological storage conditions.* International Journal of Greenhouse Gas Control, 2013. **18**: p. 75-87.
87. Bernal, S.A., E.D. Rodríguez, R. Mejía de Gutiérrez, and J.L. Provis, *Performance of alkali-activated slag mortars exposed to acids.* Journal of Sustainable Cement-Based Materials, 2012. **1**(3): p. 138-151.
88. Bakharev, T., *Resistance of geopolymer materials to acid attack.* Cement and Concrete Research, 2005. **35**(4): p. 658-670.
89. Lee, N. and H. Lee, *Influence of the slag content on the chloride and sulfuric acid resistances of alkali-activated fly ash/slag paste.* Cement and Concrete Composites, 2016. **72**: p. 168-179.
90. Yongzhi, L., *Compressive strength of masonry mortar at different curing times (砌筑砂浆在不同龄期时的硬化强度).* Architecture Technology (建筑技术), 1983(7): p. 51.

Figure 1

Click here to access/download;Figure;Figure1.tif

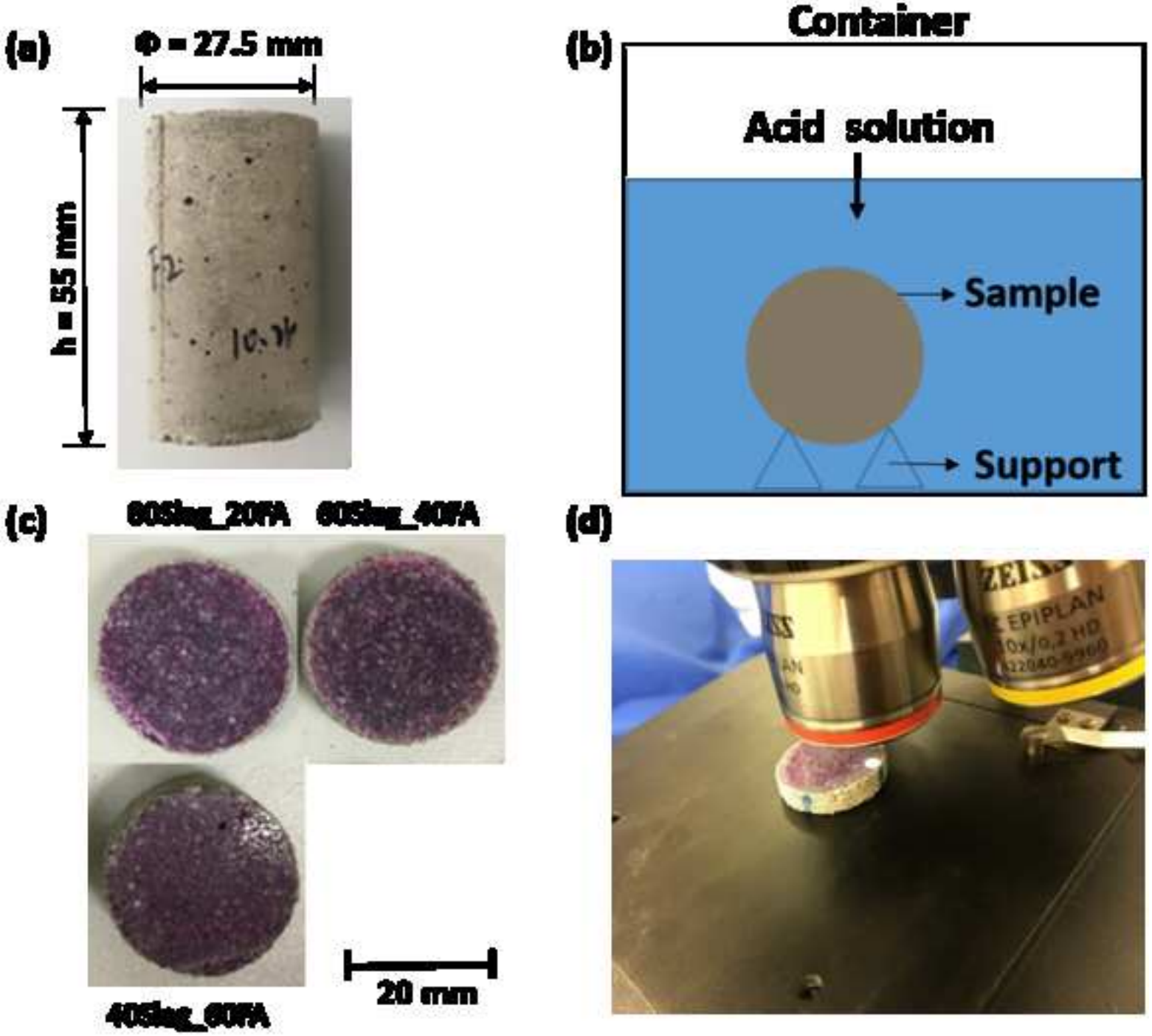


Figure 2

Click here to access/download;Figure;Figure2.tif

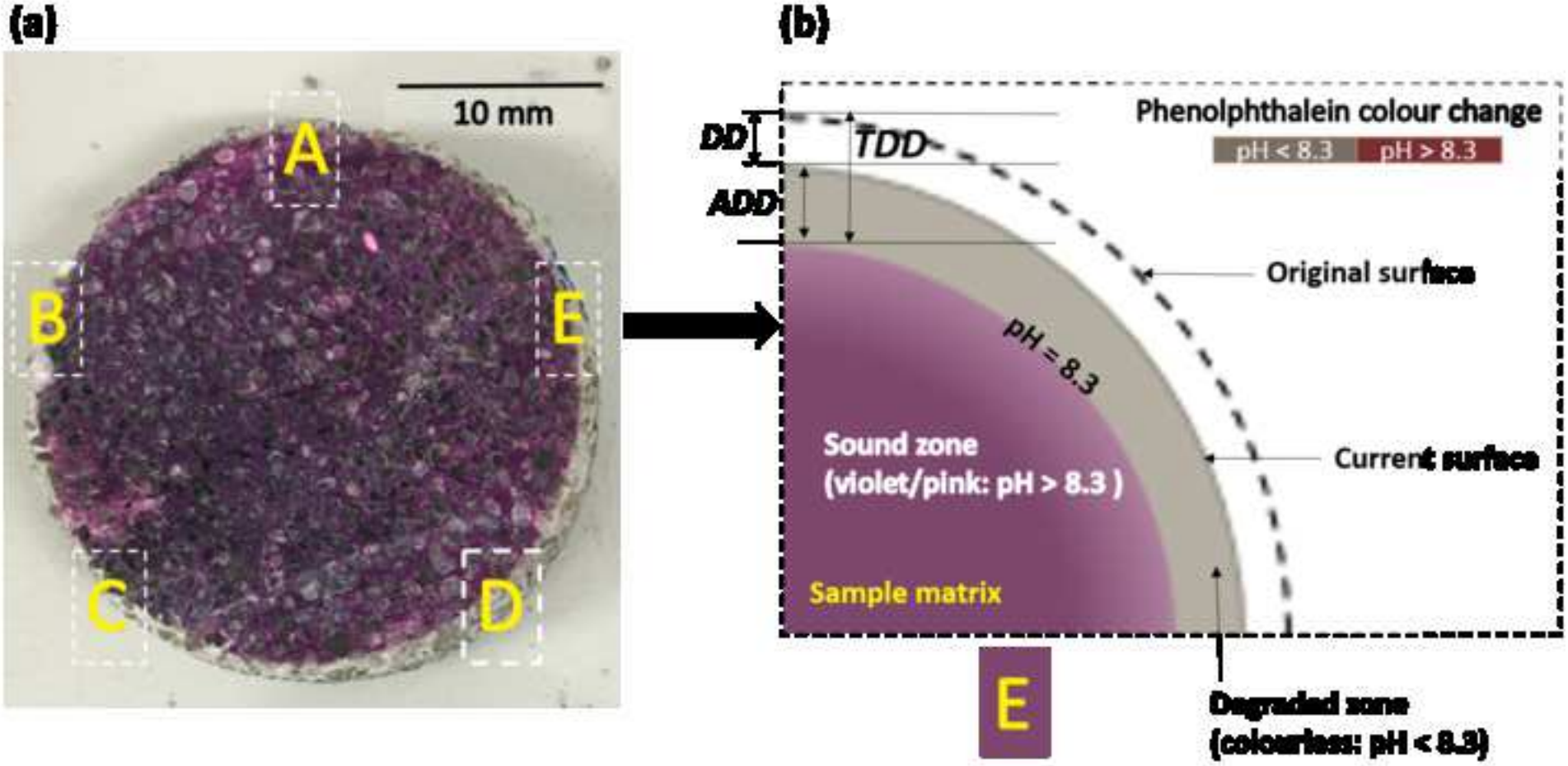


Figure 3

Click here to access/download;Figure;Figure3.tif

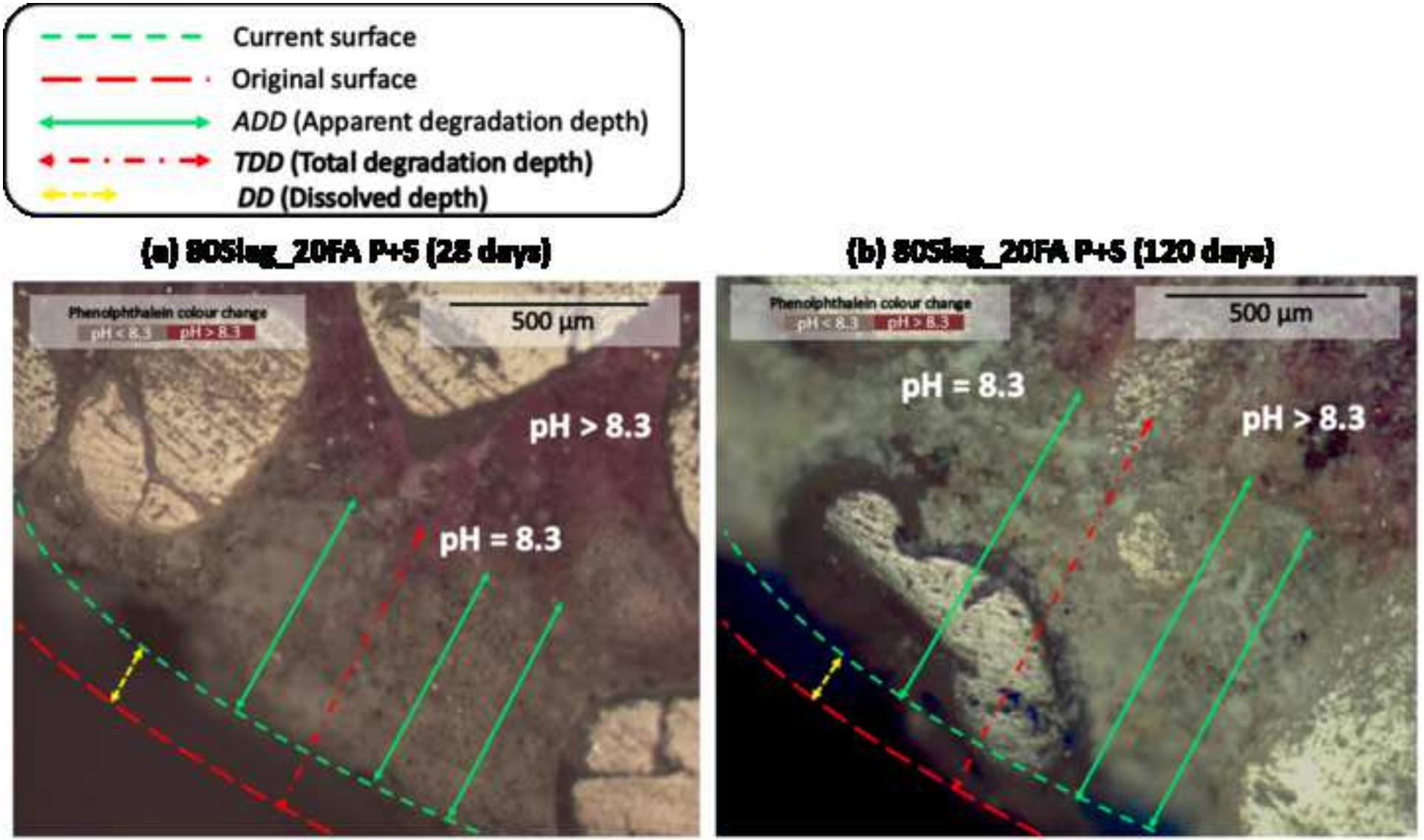


Figure 4 a

Click here to access/download;Figure;Figure4(a).tif

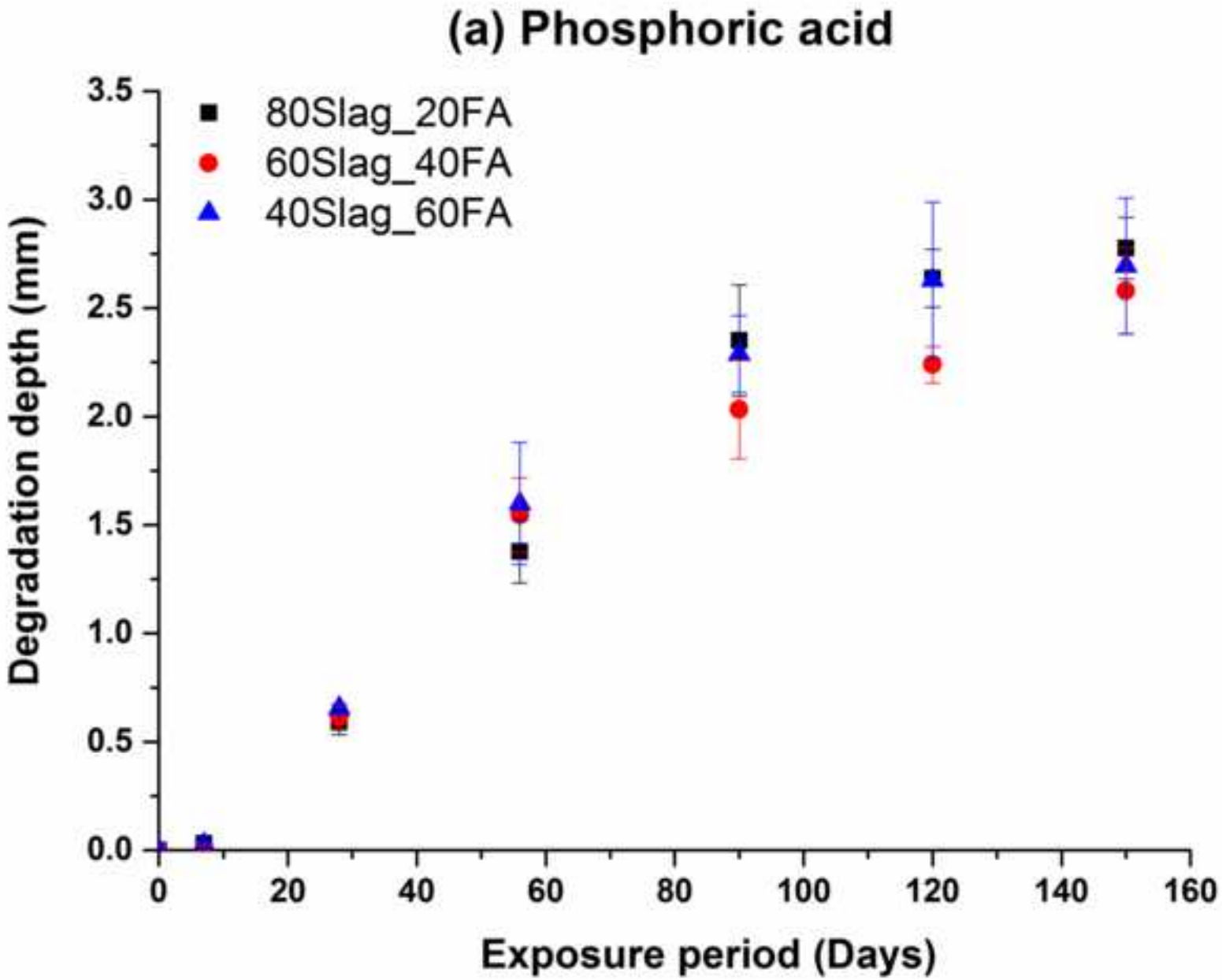
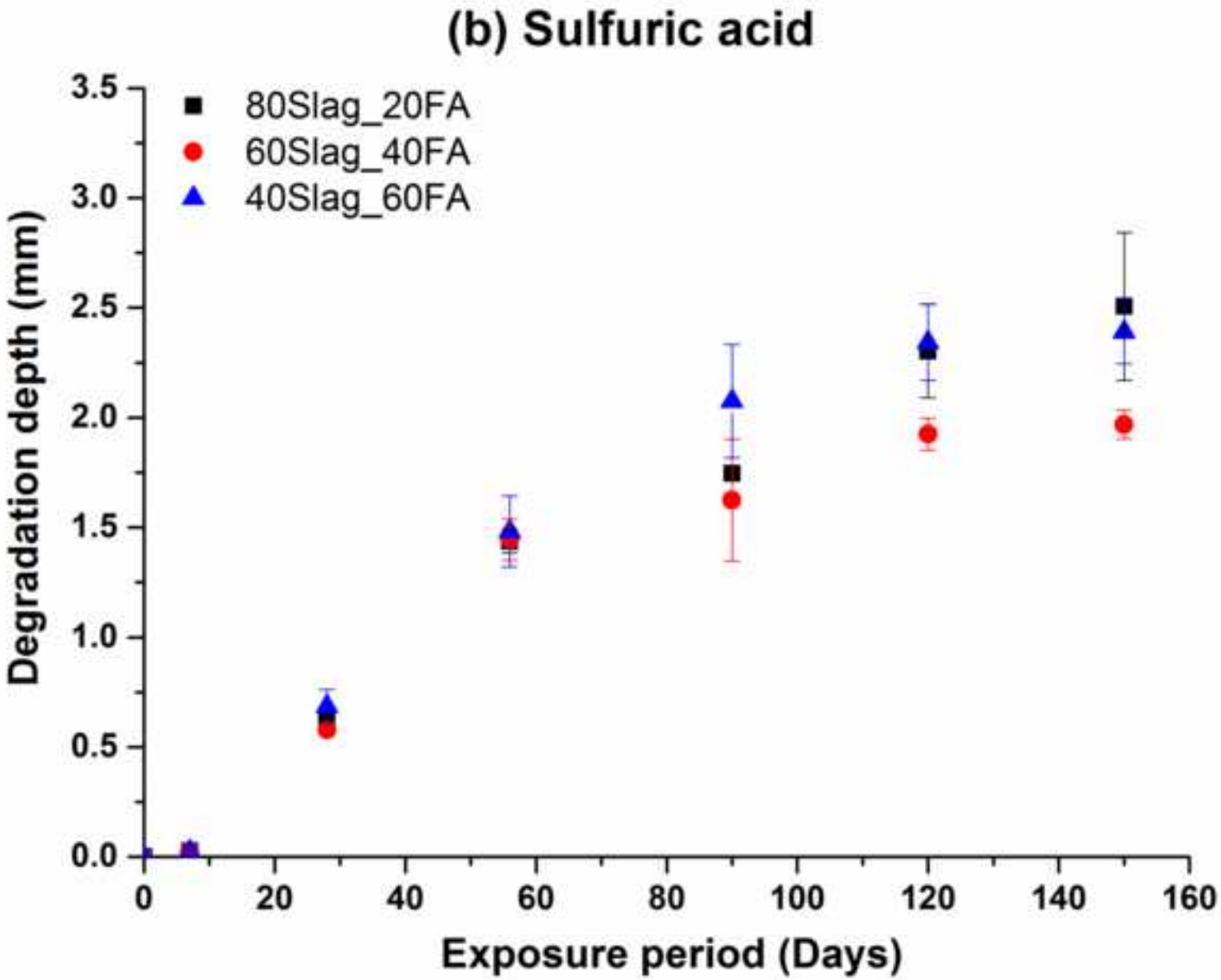


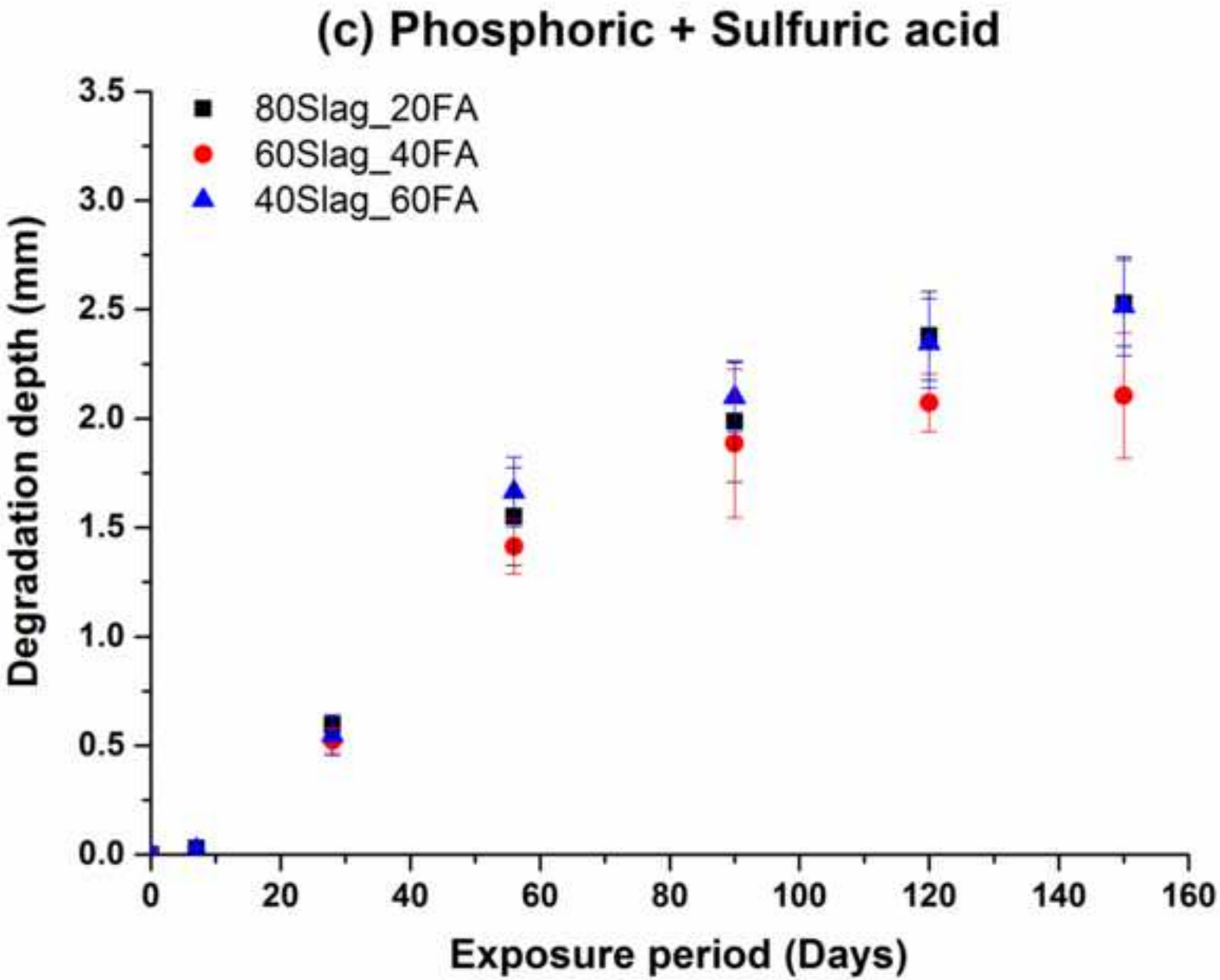
Figure 4 b

Click here to access/download;Figure;Figure4(b).tif



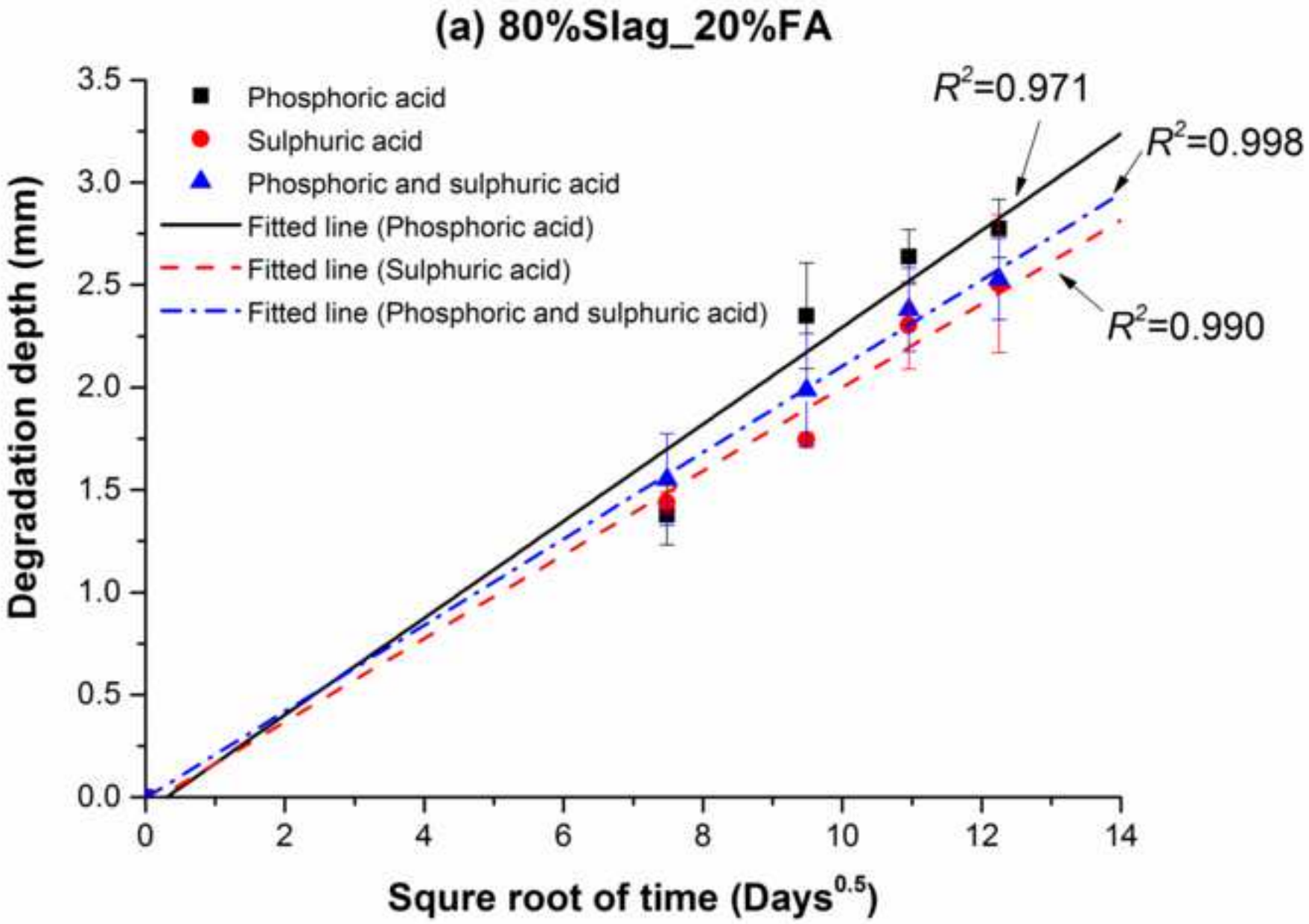
Figure

Click here to access/download;Figure;Figure4(c).tif



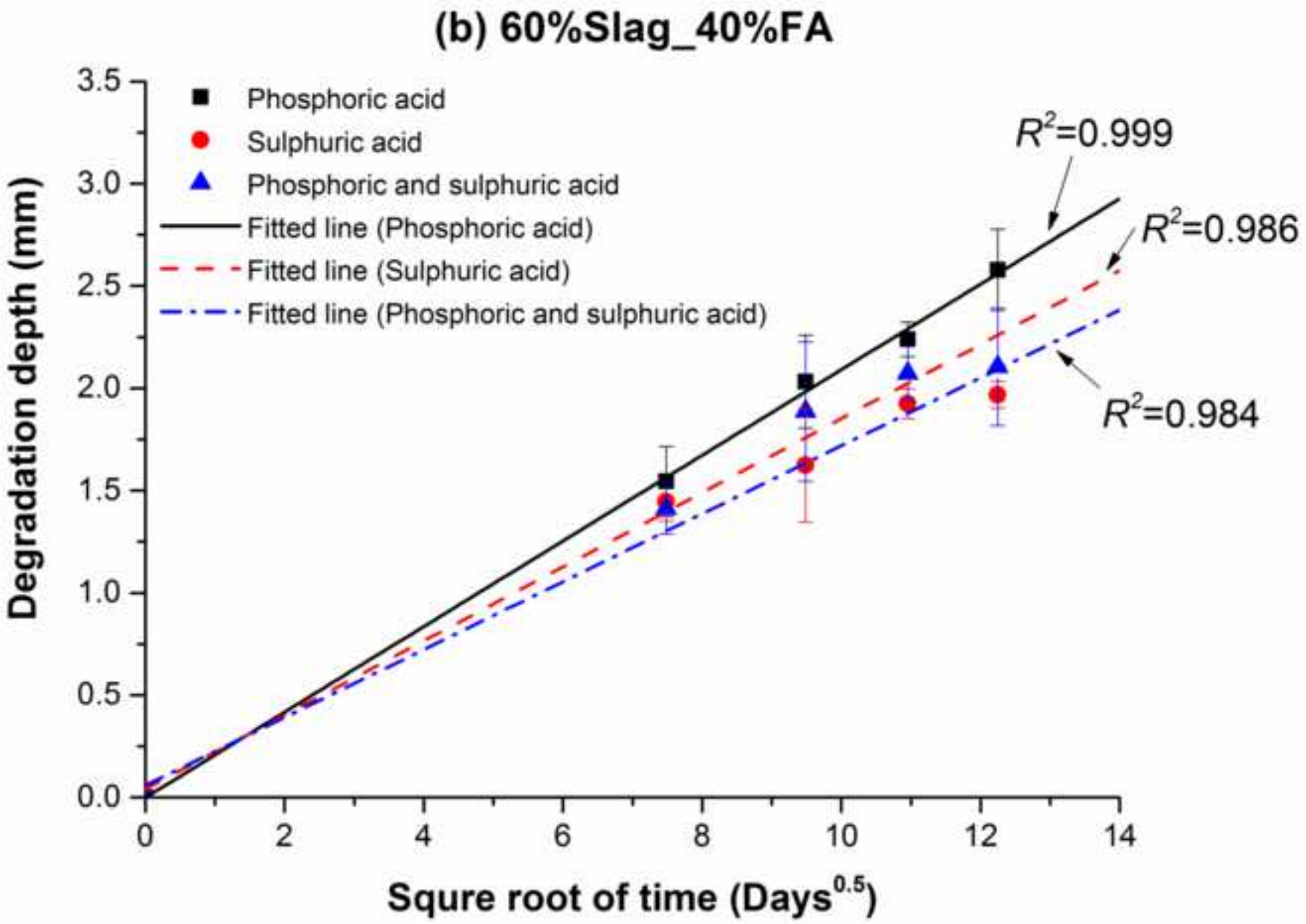
Figure

Click here to access/download;Figure;Figure5(a).tif



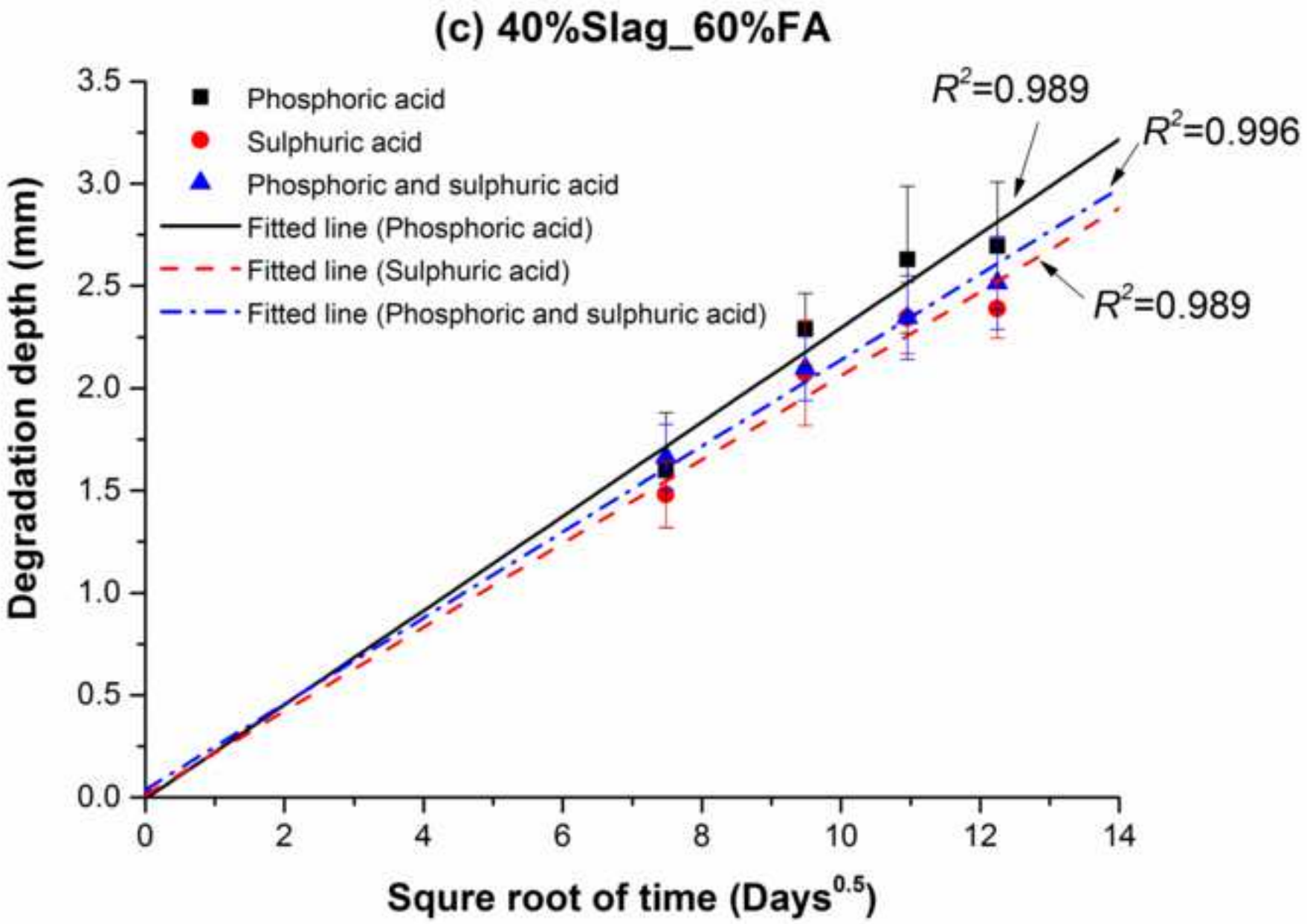
Figure

Click here to access/download;Figure;Figure5(b).tif



Figure

Click here to access/download;Figure;Figure5(c).tif



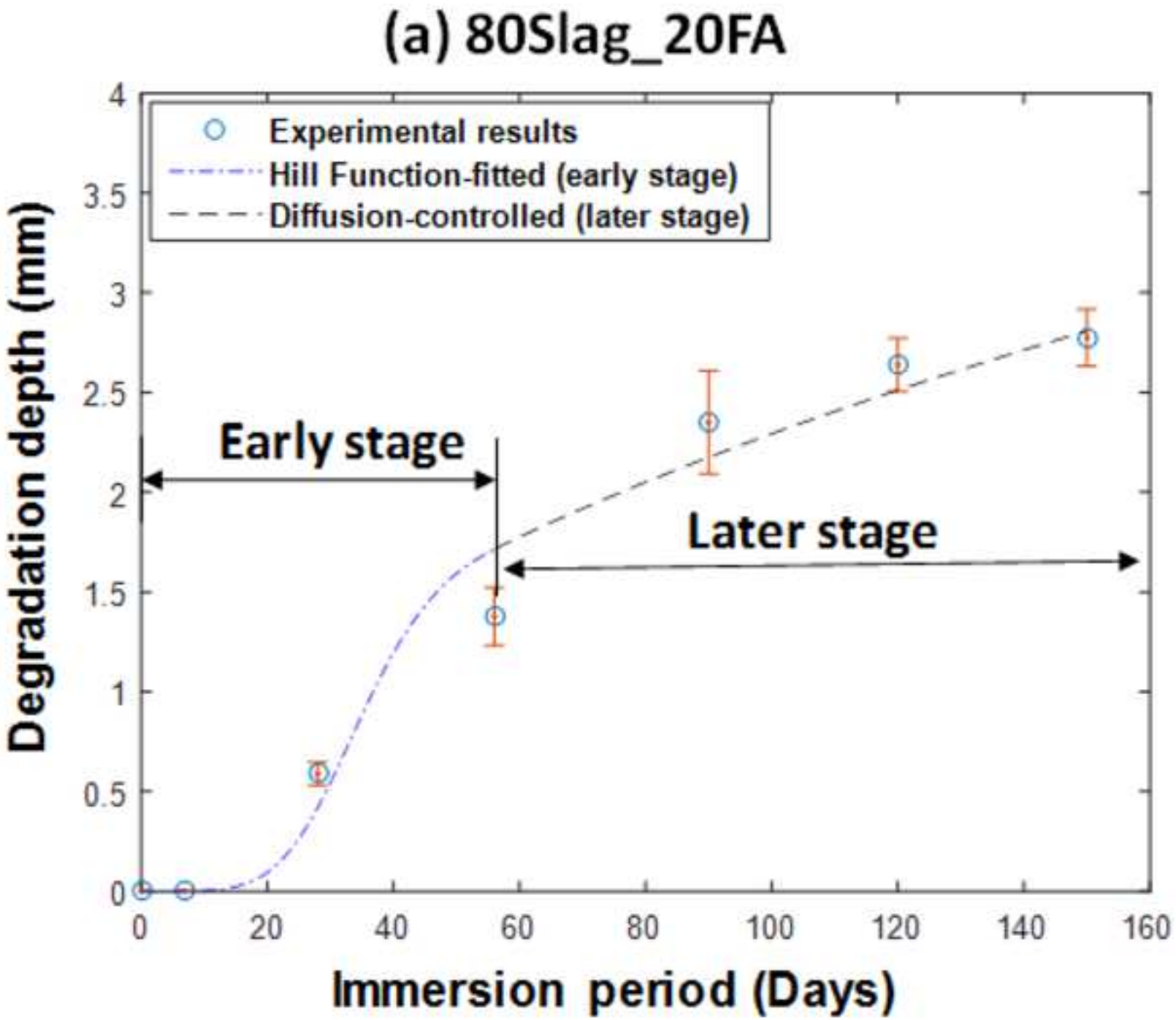
Figure

Click here to access/download;Figure;Figure6.tif



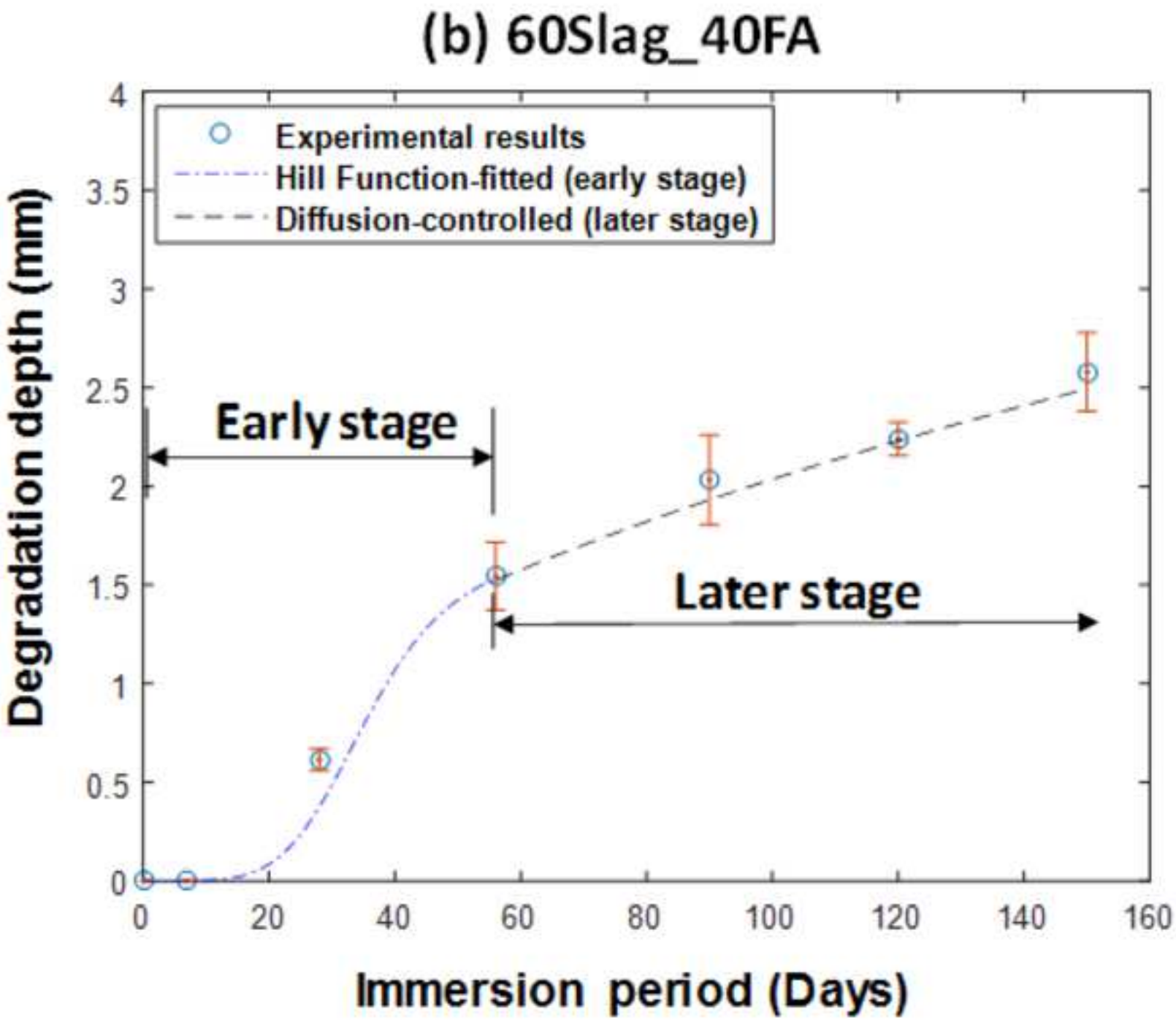
Figure

Click here to access/download;Figure;Figure7(a).tif



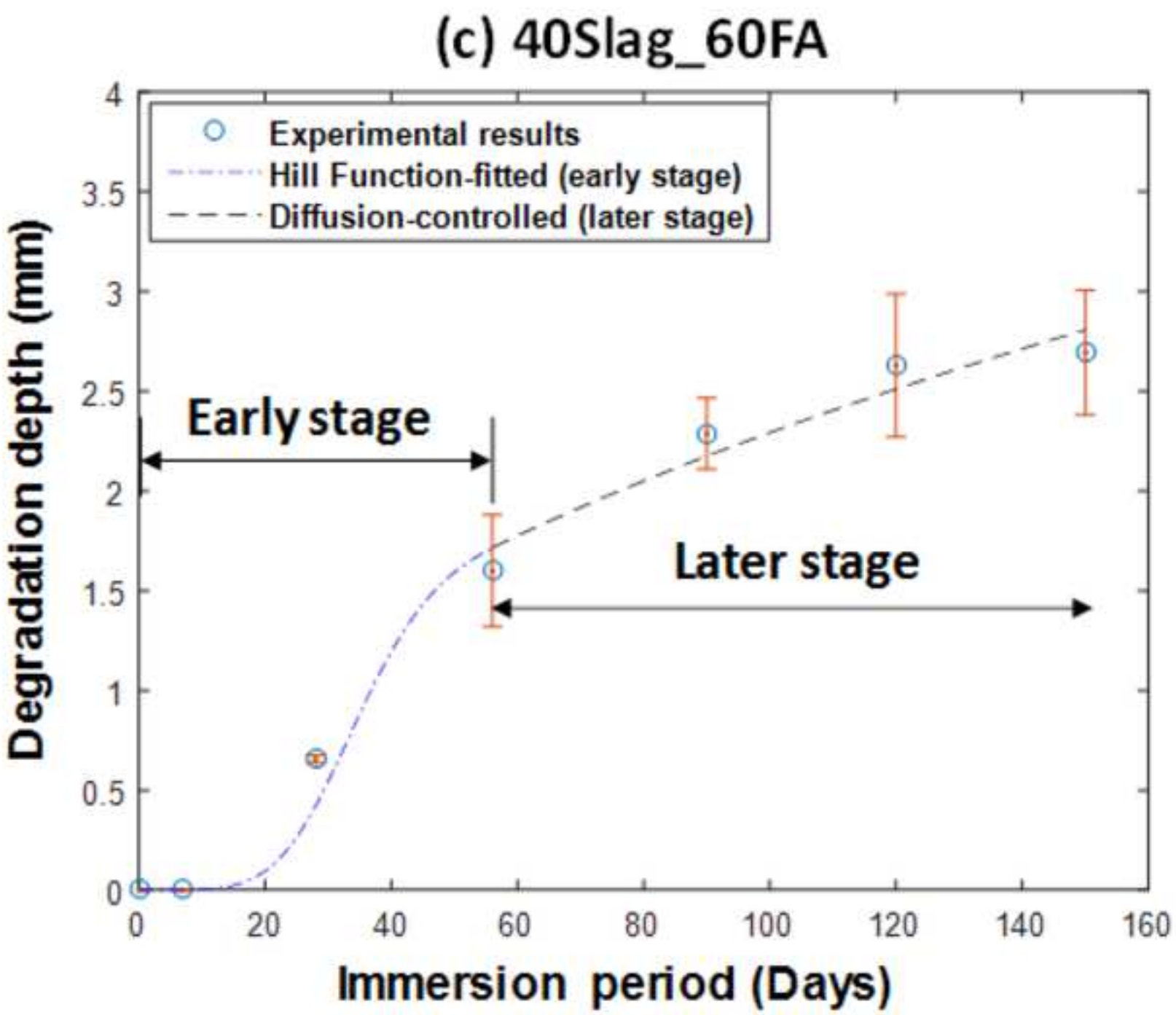
Figure

Click here to access/download;Figure;Figure7(b).tif



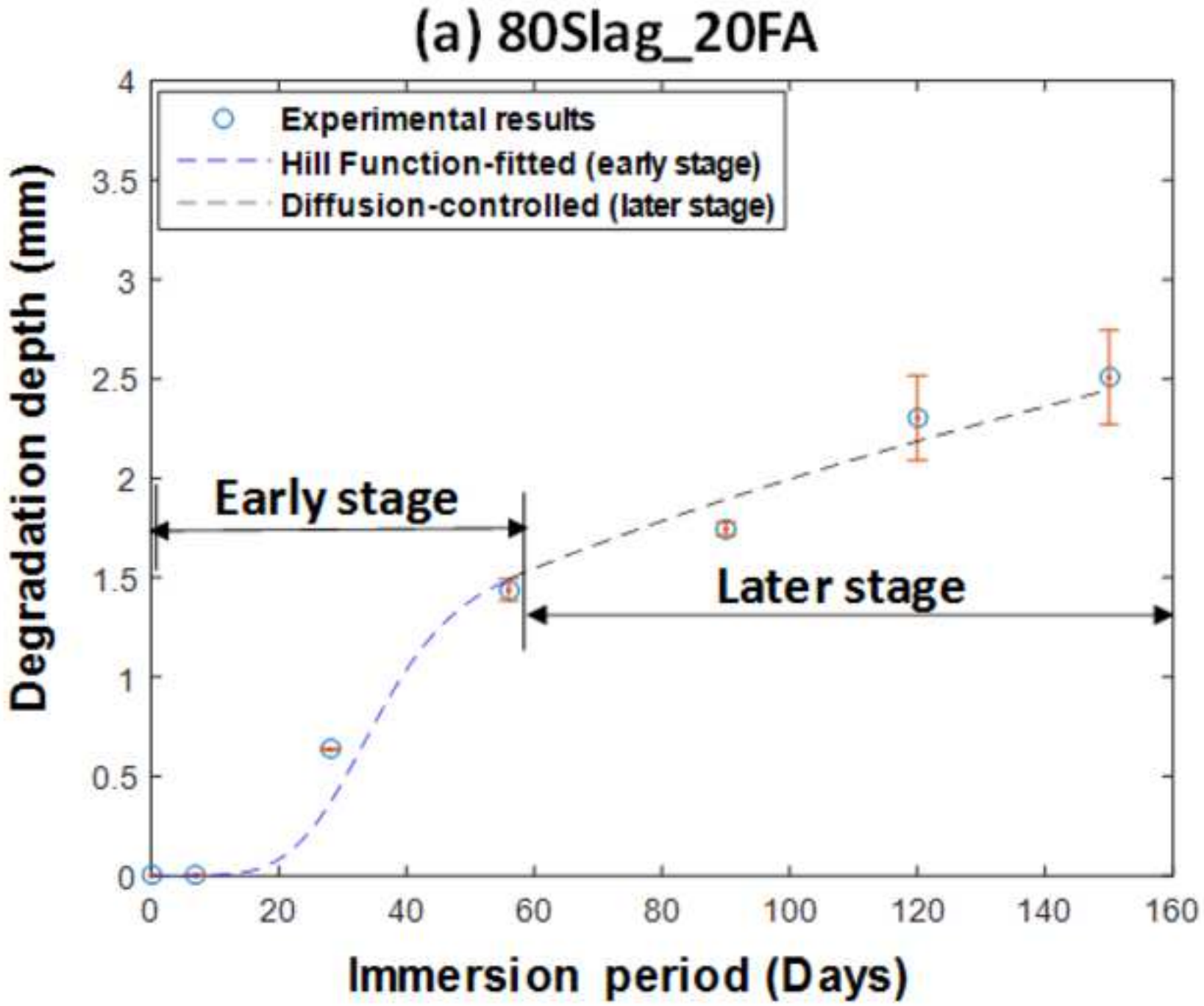
Figure

Click here to access/download;Figure;Figure7(c).tif



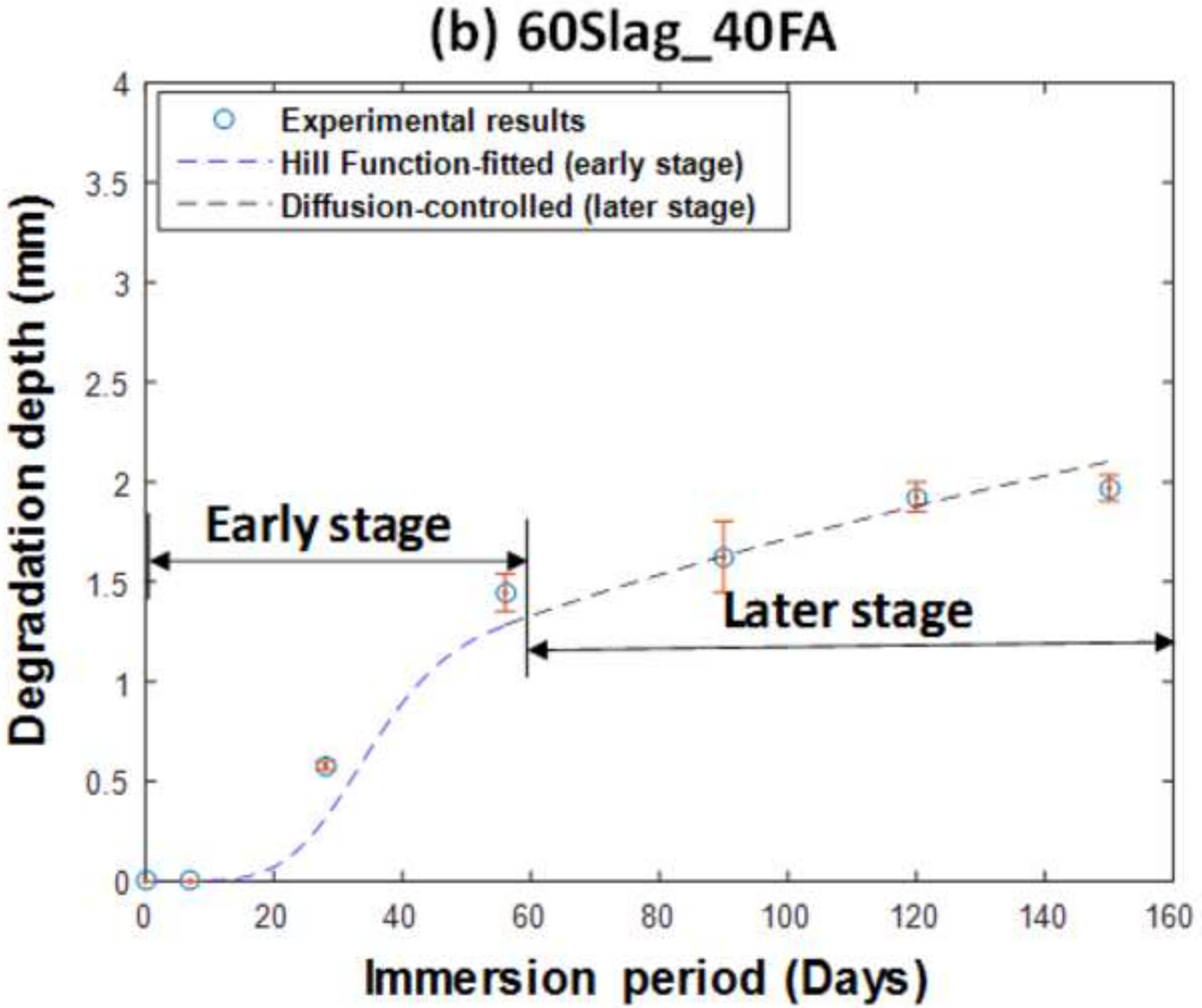
Figure

Click here to access/download;Figure;Figure8a.tif



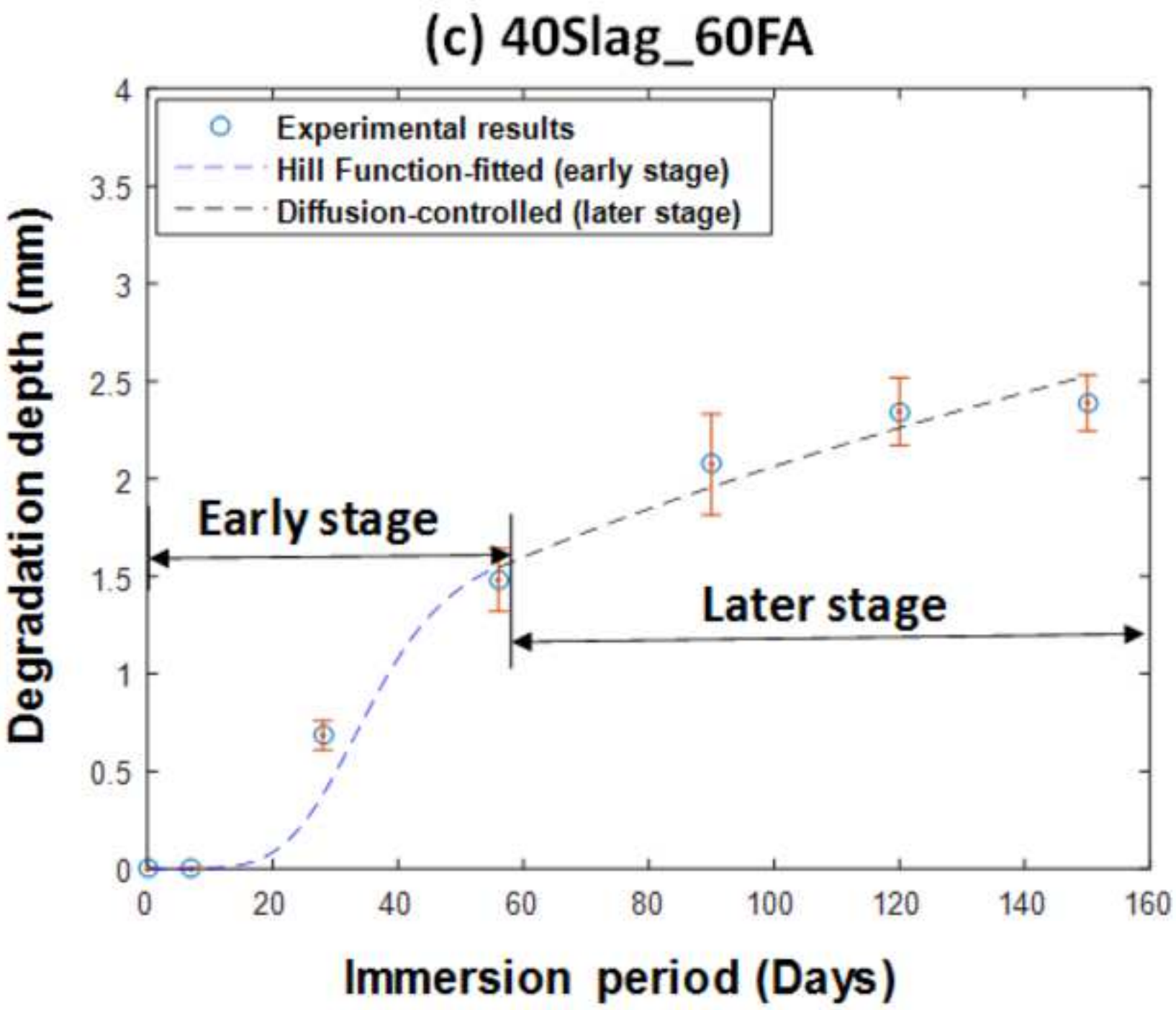
Figure

Click here to access/download;Figure;Figure8b.tif



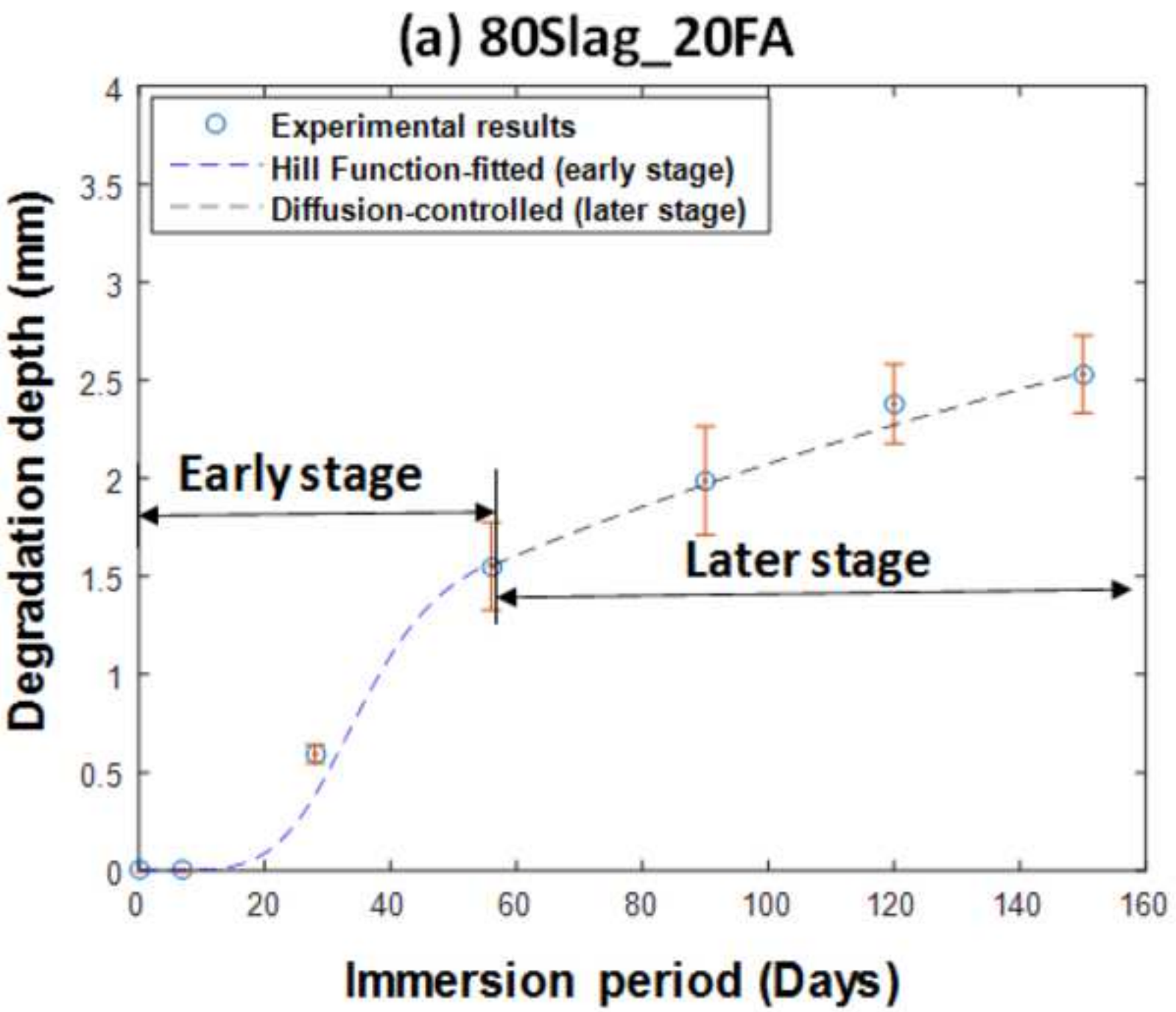
Figure

Click here to access/download;Figure;Figure8c.tif



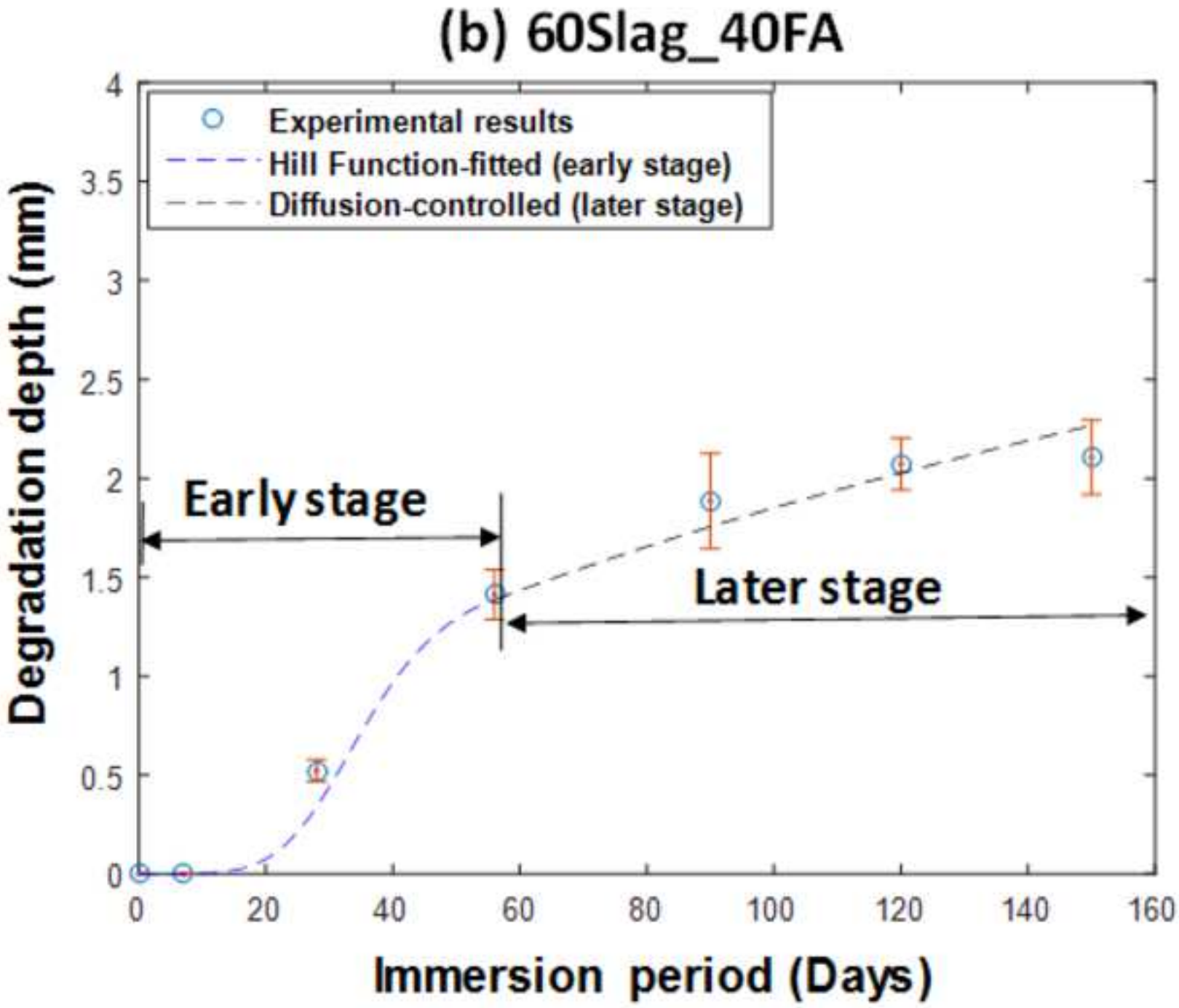
Figure

Click here to access/download;Figure;Figure9a.tif



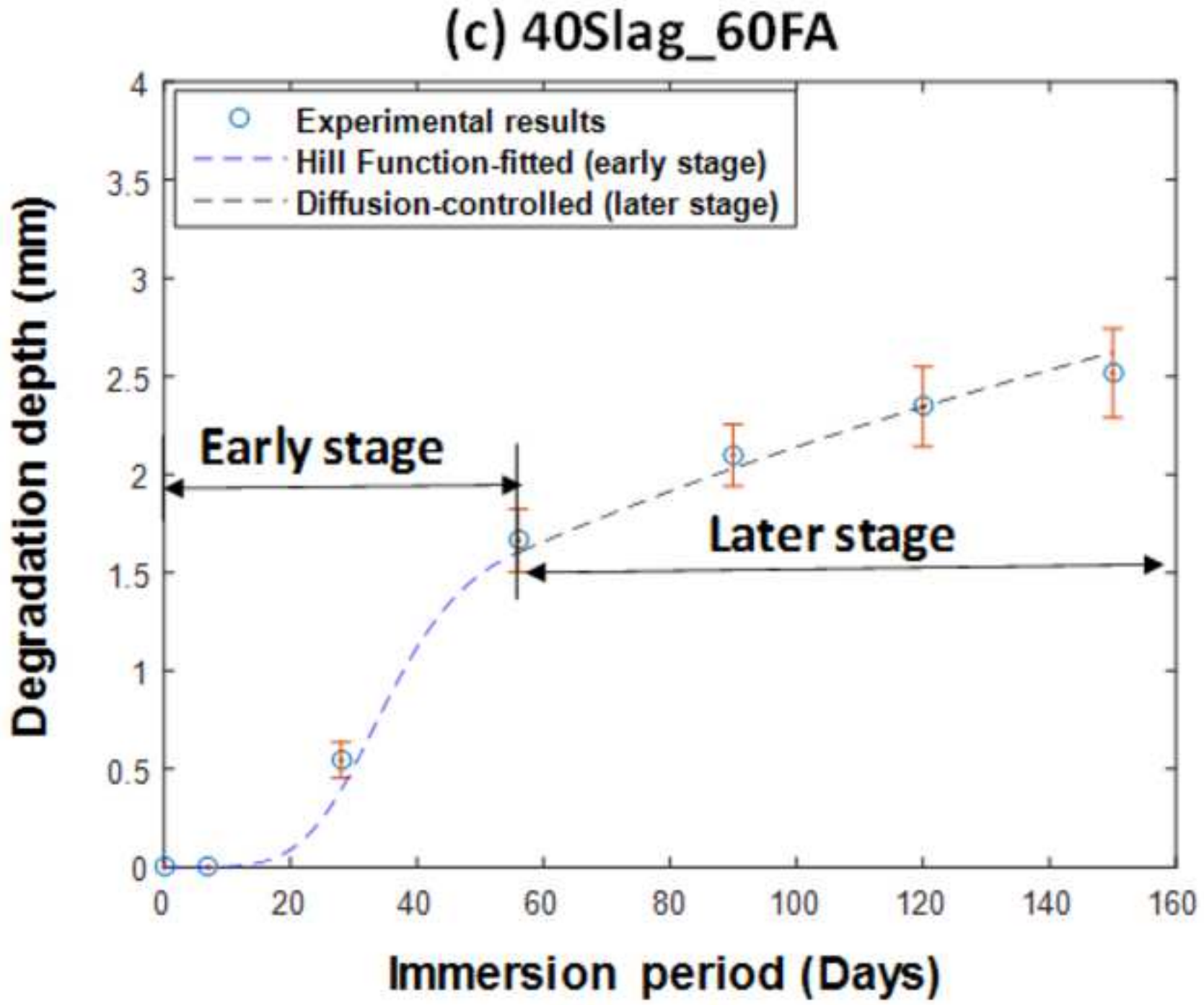
Figure

Click here to access/download;Figure;Figure9b.tif



Figure

Click here to access/download;Figure;Figure9c.tif



Figure

Click here to access/download;Figure;Figure10.tif

